New Mexico Geological Society

Downloaded from: https://nmgs.nmt.edu/publications/guidebooks/76



Sandia Orbicular Occurrences Revisited

James Stimac, Fraser Goff, and Virginia T. McLemore
2026, pp. 175-192. https://doi.org/10.56577/FFC-76.175

in:

Geology of the Albuquerque Region - Fall Field Conference 2026, Connell, Sean D.; Koning, Daniel J.;, New Mexico Geological Society 76th Annual Fall Field Conference Guidebook, 452 p. https://doi.org/10.56577/FFC-76

This is one of many related papers that were included in the 2026 NMGS Fall Field Conference Guidebook.

Annual NMGS Fall Field Conference Guidebooks

Every fall since 1950, the New Mexico Geological Society (NMGS) has held an annual Fall Field Conference that explores some region of New Mexico (or surrounding states). Always well attended, these conferences provide a guidebook to participants. Besides detailed road logs, the guidebooks contain many well written, edited, and peer-reviewed geoscience papers. These books have set the national standard for geologic guidebooks and are an essential geologic reference for anyone working in or around New Mexico.

Free Downloads

NMGS has decided to make peer-reviewed papers from our Fall Field Conference guidebooks available for free download. This is in keeping with our mission of promoting interest, research, and cooperation regarding geology in New Mexico. However, guidebook sales represent a significant proportion of our operating budget. Therefore, only *research papers* are available for download. *Road logs*, *mini-papers*, and other selected content are available only in print for recent guidebooks.

Copyright Information

Publications of the New Mexico Geological Society, printed and electronic, are protected by the copyright laws of the United States. No material from the NMGS website, or printed and electronic publications, may be reprinted or redistributed without NMGS permission. Contact us for permission to reprint portions of any of our publications.

One printed copy of any materials from the NMGS website or our print and electronic publications may be made for individual use without our permission. Teachers and students may make unlimited copies for educational use. Any other use of these materials requires explicit permission.

This page is intentionally left blank to maintain order of facing pages.

New Mexico Geological Society Guidebook, 76th Fall Field Conference, 2026, p. 175–192, https://doi.org/10.56577/FFC-76.175

SANDIA ORBICULAR OCCURRENCES REVISITED

JAMES STIMAC[1], FRASER GOFF[2], AND VIRGINA T. MCLEMORE[3]

[1]Stimac Geothermal Consulting, 342 Whiteoaks Drive NE, Albuquerque, NM 87122; sgcgeo00@gmail.com
[2]Department of Earth and Environmental Science, New Mexico Institute of Mining and Technology, Socorro, NM 87801
[3]New Mexico Bureau of Geology & Mineral Resources, Socorro, NM 87801

Abstract—We revisited two well-described occurrences of orbicular texture in the Sandia Mountains intrusive complex and propose a model for their formation. Both occurrences have limited exposure but appear to be within fault-associated dikes or pipes of monzodioritic to gabbroic magma intruding into the main-phase megacrystic quartz monzonite. The cores of orbicules are rounded feldspar megacrysts and granitic and metamorphic rocks, while their concentrically layered shells consist of coarse-grained biotite, plagioclase, and potassium feldspar (K-feldspar) with rapid-growth textures. At the La Luz occurrence, comb texture is also present at the monzodiorite contact. In the Tijeras Canyon occurrence, the host rock is a hornblende–monzodiorite, and orbs are generally large (>5 cm), with thicker outer shells consisting of plagioclase and later microcline. Aplite dikes and late-stage magmatic to hydrothermal alteration postdate orbicule formation in both cases. Ascent and emplacement of hotter, more mafic, water-saturated magma into the semisolid main-phase pluton explain aspects of host-rock and orbicular textures, such as the rapid growth of shell minerals on a resorbed substrate. Our model entails (1) mafic underplating and disruption of wallrocks to form orb core fragments; (2) entrainment and resorption of core material in an ascending, largely superheated magma with high volatile content and few crystal nuclei; and (3) rapid changes in magma/magmatic volatile composition and temperature, related to ascent, and volatile accumulation and loss, triggered by both fluid pressure decline and magmatic undercooling. We conclude that the orbicular shells formed at the magmatic–hydrothermal interface near the top of the main-phase pluton. Repeated cycles of undercooled magmatic growth of biotite, plagioclase, and K-feldspar are consistent with multiple episodes of volatile accumulation and release, or crystallization directly from an accumulated magmatic volatile phase. The association of comb layering and adjacent orbicules is consistent with their formation and accumulation at a local roof or restriction along volatile-release pathways (millimeter-scale aperture fractures) too narrow for orbs to pass through. Both localities were substantially faulted and hydrothermally altered after orb formation.

INTRODUCTION

The Sandia Mountains form a Proterozoic granitic terrain capped by Mississippian to Permian sedimentary rocks (Kelly and Northrop, 1975; Grambling et al., 2016). Here we examine late-stage features of the intrusive complex, highlighting two occurrences of orbicular texture (Fig. 1). We revisit these beautiful and fascinating rocks and speculate on their mechanisms of formation in more detail than previous studies have (Enz, 1974; Enz et al., 1979; Affholter, 1979; Affholter and Lambert, 1982). We focus mainly on field-scale and micro-scale textural and mineralogical observations, augmented by whole-rock chemistry.

The main phase of the Sandia pluton was assembled at 1437 ± 12 Ma (Gaston, 2014; Grambling et al., 2016; Holland et al., 2020). It typically ranges from quartz monzonite to granodiorite in composition and has large, commonly aligned, potassium-feldspar (K-feldspar) megacrysts (3–5 cm in diameter) in a coarse matrix of quartz, plagioclase, and biotite with or without hornblende (Table 1; Kelly and Northrop, 1975). Accessory minerals include titanite, iron–titanium (Fe–Ti) oxides, apatite, and zircon; allanite is also present in samples described in this paper.

Heterogeneities in the main-phase intrusion, comprising up to a few percent of its volume, include mafic microgranular enclaves (MME), often concentrated in swarms, and partially assimilated and reacted country-rock debris. MME formed by episodic mafic input, resulting in the mingling of mafic to hybrid intermediate magmas into the main granitoid magma body. The presence of foliated xenoliths, surmicaceous enclaves, and residual quartz indicates that assimilation of partially digested country rock was also important during magma emplacement and consolidation.

Following the main phase of intrusion, pegmatite and aplite dikes were emplaced throughout much of the pluton, but they are reportedly less abundant in the southern 4–5 km (2.5–3.1 mi) of the intrusive complex. All magmatic phases are cut by faults and fractures; some are mineralized by hydrothermal alteration (Shomaker, 1965; Kelly and Northrop, 1975). The main products of hydrothermal alteration are epidote, chlorite, quartz, titanite, sericite/muscovite, and pyrite and/or hematite. Quartz ± epidote ± chlorite is perhaps the most common megascopic vein assemblage, indicating ingress and circulation of meteoric–hydrothermal fluid with temperatures >240 °C (>464 °F; Stimac et al., 2015, fig. 46.5).

We focus on two well-documented outcrops of orbicular-textured rocks (Figs. 1–3), one in the north, referred to as the La Luz occurrence (Enz, 1974; Thompson and Giles, 1974; Enz et al., 1979), and one in the south, referred to as the Tijeras Canyon occurrence (Affholter, 1979; Affholter and Lambert, 1982). Thompson and Giles (1974) interpreted La Luz orbicules (referred to here as "orbs") as being formed by metasomatic reactions between large biotite monzonite–diorite xenolithic bodies and magmatic fluids during the crystallization of the granite. On the other hand, Enz (1974) and Enz et al. (1979) attributed them to late-stage magmatic processes. Affholter (1979) and Affholter and Lambert (1982) first described the Tijeras Canyon occurrence and likewise concluded that it had a complex origin involving late-stage igneous crystallization.

Although the fascinating phenomenon of orbicular texture is relatively uncommon, there are hundreds of documented

occurrences in granitoids worldwide (see literature summaries in Grosse et al., 2010; McCarthy and Müntener, 2016; and Díaz-Alvarado et al., 2017). Orbicular granites are defined as masses with rounded cores of granitic or metamorphic rocks or minerals overgrown by concentric shells of granitoid minerals, usually consisting of light and dark layers, and enclosed in a granitic matrix. The concentric shells may be composed mainly of a single mineral or of multiple mineral intergrowths with either a radial or concentric crystal growth habit. Orbicular horizons are commonly found as dike-like bodies or layers, a few meters to a few tens of meters thick, that may be traced for meters to tens of meters. They are commonly found at or near the margins of intrusions or in distinctly more mafic intrusive phases (e.g., Enz, 1974; Affholter, 1979; Smillie and Turnbull, 2014). Ort (1992) described the rare occurrence of orbicular volcanic rocks at Cerro Panizos, central Andes, suggesting that they formed near a caldera ring-fracture vent and an underlying magma chamber margin. His findings support theories of magmatic origins for orbs, as documented above, suggesting that rhythmic layering can occur in volcanic systems along pathways of volatile loss and eruption.

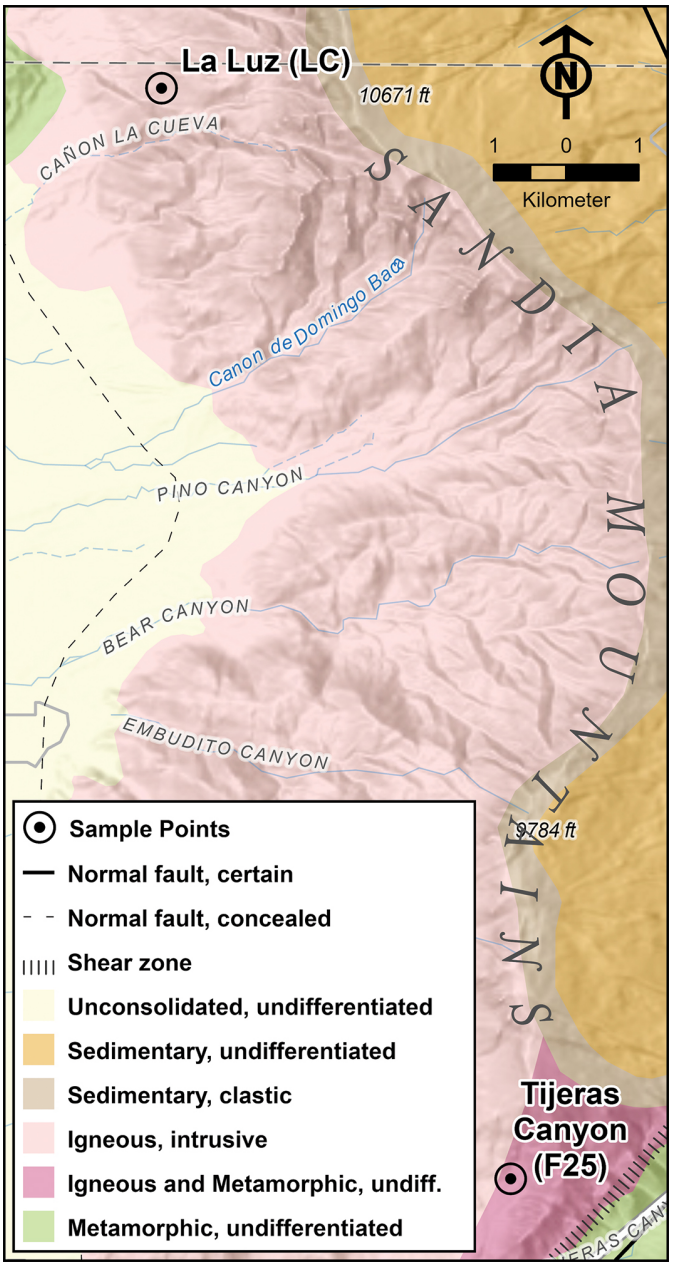


FIGURE 1. Location map for Sandia Mountains intrusive complex and orbicular occurrences.

Some orbicular occurrences (including the La Luz occurrence; Enz, 1974) are associated with comb layering (Moore and Lockwood, 1973), a type of unidirectional solidification texture (UST). Comb layering is characterized by elongated, branching minerals growing from a pluton or dike wall. The elongate growth direction of crystals is typically perpendicular to the layering, forming centimeter- to meter-thick banded sequences (Leveson, 1966; Moore and Lockwood, 1973; McCarthy and Müntener, 2016). Growth textures that define orbicular rocks have essentially the same unidirectional characteristics as comb layers but are deposited on free-floating seeds (e.g., rounded xenoliths, enclaves, or feldspar megacrysts) rather than on an intrusion wall or roof. In the broadest sense, monomineralic plagioclase shells on K-feldspar (rapakivi texture) may also be considered a type of UST.

The term UST is used primarily by economic geologists, who focus on the role of accumulated magmatic fluid at apices in highly evolved intrusions that might host ore deposits (Lowenstern and Sinclair, 1996; Seo et al., 2021; Bain et al., 2022; Müller et al., 2023). The dominant UST mineral in these examples is quartz, locally interlayered with fine-grained granite or aplite. In examples of comb-layering associated with orbicular rocks, the main mineral phase is typically plagioclase, layered with biotite or other ferromagnesian minerals (McCarthy and Müntener, 2016), and most models for their formation invoke crystallization from a water-rich magma (Lahti, 2005; Sylvester, 2011; McCarthy and Müntener, 2016; Díaz-Alvarado et al., 2017). However, Moore and Lockwood (1973) inferred crystallization from a magmatic fluid, and Sylvester (2011) also entertained this possibility. Certainly, the formation of comb-layered and orbicular rocks is one of several hallmarks of the magmatic–hydrothermal interface at or near the tops of mostly consolidated plutons.

FIELD RELATIONSHIPS, ROCK TYPES, AND TEXTURES

We build on detailed descriptions of Sandia orbicular occurrences by Robert David Enz, Kathleen Affholter, and colleagues, made about 50 years ago. The striking orbicular-textured rocks that comprise the La Luz and Tijeras Canyon occurrences have many similarities and a few differences that can be observed at the outcrop (meter to centimeter scale; Figs. 4 and 5) and thin-section scales (centimeter to micron scale; Figs. 6–9). We review the characteristics of the two occurrences, describing aspects of each in more detail.

La Luz Orbicules

The La Luz occurrence consists of accumulations of orbs in several outcrops forming one or more dike- or pipe-like intrusions of biotite monzodiorite to gabbro enclosed in the main-phase Sandia megacrystic granite to granodiorite (Figs. 2 and 4). Aplite dikes postdate orb formation but are too thin and poorly exposed to map (Fig. 4D). Full thin-section images of the main-phase Sandia granite and the more mafic intrusions hosting orbicular bodies are shown in Figure 6.

Enz (1974) and Enz et al. (1979) made a detailed study of two of the La Luz orbicular occurrences (35°13′04″ N, 106°29′30″ W and 35°13′49′″ N, 106°39′42 W; 2 km [1.25 mi] away at N33°W from the original site). They summarized the initial discovery of these occurrences and ideas on their origin. Their field maps, photographs, and detailed descriptions are a valuable resource because the current state of the outcrops has been degraded by intensive sampling.

Enz and colleagues also obtained wet chemical analyses of the orbicules and surrounding rocks. They believed that the biotite monzodiorite to gabbro was a "magmatic segregation that coexisted with the Sandia granite melt." Enz proposed an igneous crystallization origin for the orbs based on (1) normal zoning of plagioclase shells; (2) identical shell layering and mineralogy within each orbicule type (he defined four gradational types); (3) consistent plagioclase composition (An_{31}) of the outermost shell regardless of orbicule type; (4) age data; and (5) liquid-like, deformational features found in one type of orbicular rock.

Although exposures are currently poor, Enz (1974) described the contact between the main-phase granodiorite and biotite monzodiorite to gabbro as either gradational over

TABLE 1. Sample descriptions and modes.

Sample	Description	Primary rock textures	Minerals (vol%)								
			Qtz	Kfsp	Plag	Bt	Am	Ox	Tnt	Acc	PS/Alt
La Luz occurrence											
LC-03	Small orb (3 x 4.5 cm) assoc. w/ monzodiorite	Bt diorite core (1.5 x 2.5 cm) with shells of Plag and minor Bt, Plag, Bt altered to chlorite. Cut by later Qtz-feldspar-sericite veinlets.	7	3	79	5	0	1.0	0.0	0.8	4.5
LL-04	Sandia diorite	Cr gr Bt diorite, minor myrmekite, granulation, and late, cavity-filling Qtz is strained/crenulated along grain boundaries with alteration.	14	31	35	14	0	1.2	0.0	1.6	3.2
LL-08	Biotite monzodiorite to gabbro hosting orb zone	Med gr Qtz-Bt monzodiorite to Bt gabbro host rock for orbs. Qtz fills late cavities. Qtz, Bt show deformation features.	5	13	26	46	0	2.7	3.0	2.0	2.4
LL-13	Inter-orb matrix and parts of two small orbs	Matrix is fn gr microgranular. Early Plag, apatite, and Bt are encapsulated in Kfsp. Qtz fills late cavities.	8	8	54	24	0	0.5	2.0	1.2	2.3
LL-13	IOM	Fn gr equigranular texture similar to aplite	20	53	14	8	0	0.7	1.0	2.5	0.8
LL-13	Two small multi-shelled orbs	Fn gr layers of Bt and Plag with final radial textured Plag shells	6	2	59	28	0	0.1	3.1	1.0	0.8
LL-16	Small ellipsoidal orb (2.2 x 5 cm) assoc. w/ monzodiorite.	Orb shells consist of alternating acicular cr gr Bt, Plag, and Plag-Bt. Bt is mostly annular; Plag is radial. IOM is fn gr and myrmekitic. Mode refers to orb only.	6	3	60	27	0	0.1	2.1	1.3	0.5
Tijeras Canyon occurrence											
F25-06	Leucocratic aplite dike cutting orb host rock	Fn gr equigranular texture, minor myrmekite	30	42	24	2	0	0.8	0.1	1.0	0.1
F25-08	Fn gr Amp-Bt quartz monzodiorite host rock	Fn gr Amp-Bt-quartz monzodiorite host for orbs	3	15	26	22	27	2.1	3.8	1.0	0.1
F25-09	IOM	TS is mainly IOM w/ outer microcline shell; outer shell is 88% microcline, 15% Qtz, 2% other. Mode for IOM.	32	13	43	9	0	1.6	0.5	0.8	0.1
F25-11	Single-shelled orb w/ monzodiorite core, minor IOM	TS consists mainly of cellular Plag and microcline shells with minor amounts of Bt-rich core	15	31	45	4	1	1.0	1.8	0.7	0.5
F25-12	Single-shelled orb w/ monzodiorite core, minor IOM	TS consists of equal parts core, Plag shell, microcline outer shell	10	41	25	18	0	2.2	2.0	0.8	1.0

Notes: La Luz: 27 03655831, 3897836; Tijeras: 27 0369567, 3882727 (UTM NAD27); approximate mineral percentages from visual estimates. Assoc. = associated; w/ = with; Qtz = quartz; Kfsp = potassium feldspar; Plag = plagioclase; Bt = biotite; Amp = amphibole; Ox = iron-titanium oxide; Tnt = titanite; Acc = accessory minerals; IOM = inter-orb matrix; PS/Alt = pore space and alteration; cr gr = coarse grained; med gr = medium-grained; fn gr = fine-grained. Accessory minerals include zircon, apatite, allanite, and rare monazite.

1–2 m (3.3–6.6 ft) or interfingering. The biotite monzodiorite to gabbro is heterogeneous, with varying grain size and presence and alignment of megacrysts. At the outcrop scale, biotite content varies from <30% to >50%. It also contains disrupted comb-layered fragments, as well as more abundant schlieren, MME, and xenoliths (mainly surmicaceous enclaves) than the adjacent main-phase granite. These compositional and textural variations indicate that the orb host rock is a hybrid or mixed magma that also assimilated country rock, at its source or as it ascended. Assimilation appears to be a secondary process as most orb cores are granitic rather than metamorphic.

The orbs consist of round to elliptical cores surrounded by one or more shells consisting mainly of plagioclase and biotite.

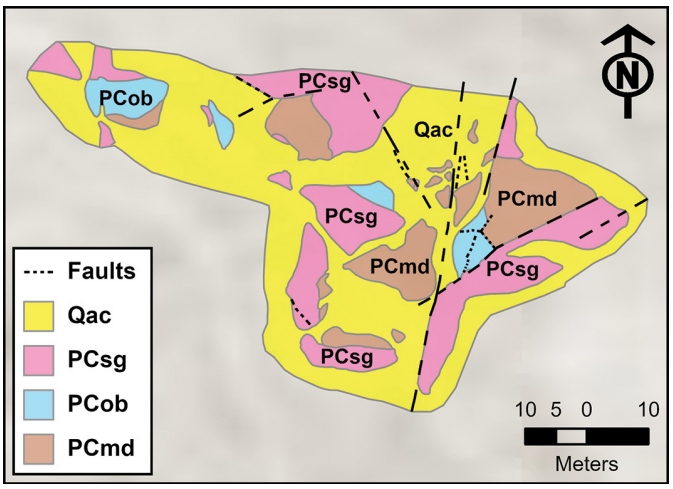


FIGURE 2. Geologic sketch map of the La Luz orbicular occurrence with main rock types (simplified from Enz, 1974). Qac = Quaternary colluvium; PCsg = Precambrian main-phase Sandia granite; PCob = Precambrian orbicular rock; and PCmd = Precambrian monzodiorite.

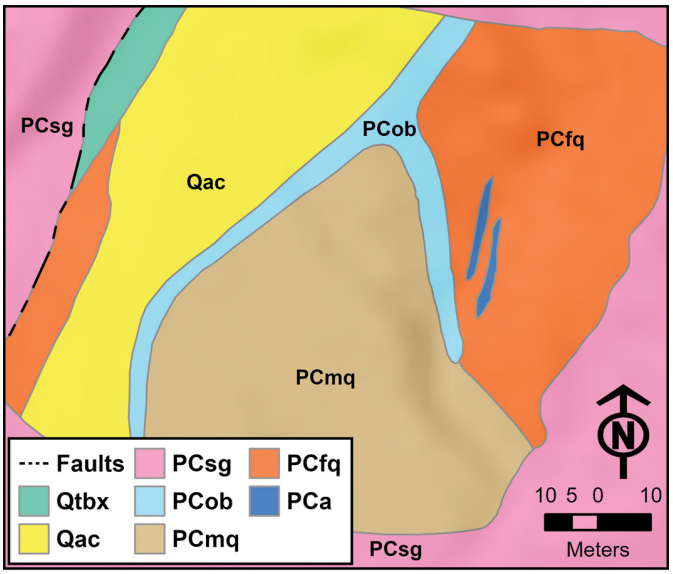


FIGURE 3. Geologic sketch map of the Tijeras Canyon orbicular occurrence with main rock types (modified from Affholter and Lambert, 1982). Qac = Quaternary alluvium and colluvium; QTbx = fault breccia; PCa = Precambrian aplite; PCob = orbicular rocks; PCfq = fine-grained quartz monzodiorite; PCmq = medium-grained quartz monzodiorite; and PCsg = Precambrian Sandia granite.

Core types include feldspar megacrysts (25%), normal granodiorite (40%), biotite monzodiorite (30%), and country rock material (5%), as determined by outcrop observations and cutting open approximately 40 orb specimens. Small orbs form more abundantly on K-feldspar megacrysts (40% for small orbs), whereas large orbs are more likely to form on granitoid or metamorphic material. Overall, this indicates significant mixing of normal megacrystic granitic material into the more mafic orb-bearing magma. Neither the hosting main-phase Sandia granite or the more mafic orb-hosting magma show foliation, although both show signs of having been locally sheared by later structural deformation.

The concentric shells of orbs consist of layered, coarse-grained biotite, interlayered fine-grained biotite–plagioclase intergrowths, and coarse-grained plagioclase (Fig. 4). Biotite in the cores is randomly oriented, whereas the shells show layers with both concentric and radially oriented biotite crystals (Thompson and Giles, 1974; Figs. 4 and 7). The initial coarse-grained biotite shell is mainly concentric, whereas the biotite–plagioclase intergrowths are mainly radial.

In the La Luz occurrence, the main shell minerals (biotite and plagioclase) display bladed growth textures inferred to indicate rapid growth in an undercooled environment (e.g., Vernon, 1985). Plagioclase compositions of the orb shells show them to be normally zoned, the innermost shell being An_{35} and the outermost shell An_{31} (Enz, 1974).

Enz (1974) documented that a few orbs experienced late brittle fracture of shells or plastic deformation against earlier, possibly more fully solidified orbs (e.g., Figs. 4A and 4B). Some shells appear to have fractured or delaminated, and inter-orb matrix (IOM) crystallized within the fractures from infiltrating liquid. He also speculated that the ellipsoidal shape of most orbs may be related to deformation. The fracturing and deformation of orb shells are consistent with their late residence in a dynamic flow environment rather than in a static crystallization environment. Diffuse late-stage copper mineralization as coatings and small accumulations is also present at the La Luz occurrence (Enz, 1974).

As described by Enz (1974), parallel to this north contact there were discontinuous layers of plagioclase (An_{31}; ~1–2 cm thick) and magnetite (3–7 mm thick) offset from the Sandia granite by a few centimeters. The feather-like plagioclase crystals or lamellae were arranged perpendicular to the layering. These crystals branched out into the orbicular matrix, away from the granitic wallrock (Enz, 1974, figs. 7 and 8), and thus are an example of comb layering as described by Moore and Lockwood (1973). In some instances, two plagioclase layers were present, ~3 cm apart (Enz, 1974, fig. 8). Associated with this layering was a biotite schlieren that not only separated the two plagioclase layers but surrounded all layering as well as the contact. The biotite, floating in a matrix of plagioclase, quartz, and microcline, was oriented with the c-axes of the crystals, perpendicular to the contact and the comb layering. These textures provide compelling evidence for UST mineral growth at the contact between the main-phase granite and monzodiorite hosting the orbs. It has been noted in most orbicular occurrences that shells consist of coarse-grained bladed

minerals that grew perpendicular to the core contact, consistent with rapid, undercooled growth conditions (Vernon, 1985). We describe small orbs in thin section that clearly demonstrate this (Figs. 4 and 7).

Tijeras Canyon Orbicules

The Tijeras Canyon orb site is in the southern Sandia Mountains pluton, not far north of the Tijeras fault and shear zone (Kirby et al., 1995). This site occupies a small hill ~30 m (~98 ft) high on a low northwest-trending ridge east of the Three Guns hiking area. The geology of the orb site is complex, comprising a near-rectangular orbicular-bearing block of about 150 m x 150 m (492 ft x 492 ft) surrounded by the main-phase Sandia granite (quartz monzonite), which is coarse grained and contains conspicuous pink megacrysts of microcline (Fig. 3; Affholter and Lambert, 1982). The block is faulted on the west side. Contact relations on other sides are poorly exposed, although rocks within the block appear to be intrusive within the main-phase Sandia pluton.

The orb zone consists of two dikes up to 5 m (16 ft) wide that partially surround a mass of dark-colored, medium-grained quartz monzodiorite (mQd). The west dike is curved and its northern part strikes 230°. The two dikes appear to join on the north side of the mQd. Fine-grained quartz monzodiorite (fQd) occurs on the east side of the east orbicular dike, and the two types of monzodiorite are in contact beyond the southern termination of the east dike. Isolated <1-m (<3.3-ft)-wide zones of pelitic schist are also found within fQd. The fQd is also found as a poorly exposed band on the east side of the fault mentioned above and as tiny "islands" poking out of colluvium. A thin (<0.5-m [<1.6 ft]) dike of fQd was found cutting the Sandia granite beyond the area shown by Figure 3.

Two aplite dikes (both striking ~215°) cut the fQd east of the east orb dike. Aplite and pegmatite dikes also cut the main-phase Sandia granite surrounding the orbicular-bearing block. The rocks are locally hydrothermally altered to an epidote–chlorite–adularia–quartz assemblage appearing in both veins and groundmass.

The Tijeras orb-bearing dikes are spectacular, consisting of bright pink microcline shells up to 15 cm (6 in) or more in diameter, generally surrounding inner shells of plagioclase (Fig. 5). The cores consist of granitic country rock (Sandia granite), K-feldspar megacrysts, both granite and megacrysts, and what appears to be biotite-rich schist or gneiss (surmicaceous enclaves). The orbs are sometimes plastically deformed or "squashed." IOM is pale-gray, fine-grained biotite-bearing aplitic material, although the texture of the infilling is not uniform. Thin aplite dikes also cut the orbicular dikes (Fig. 5D). In the northwest area of the joined dikes, two orb-rich zones are separated by a band or dike of aplitic material ~30–40 cm (~12–16 in) in width.

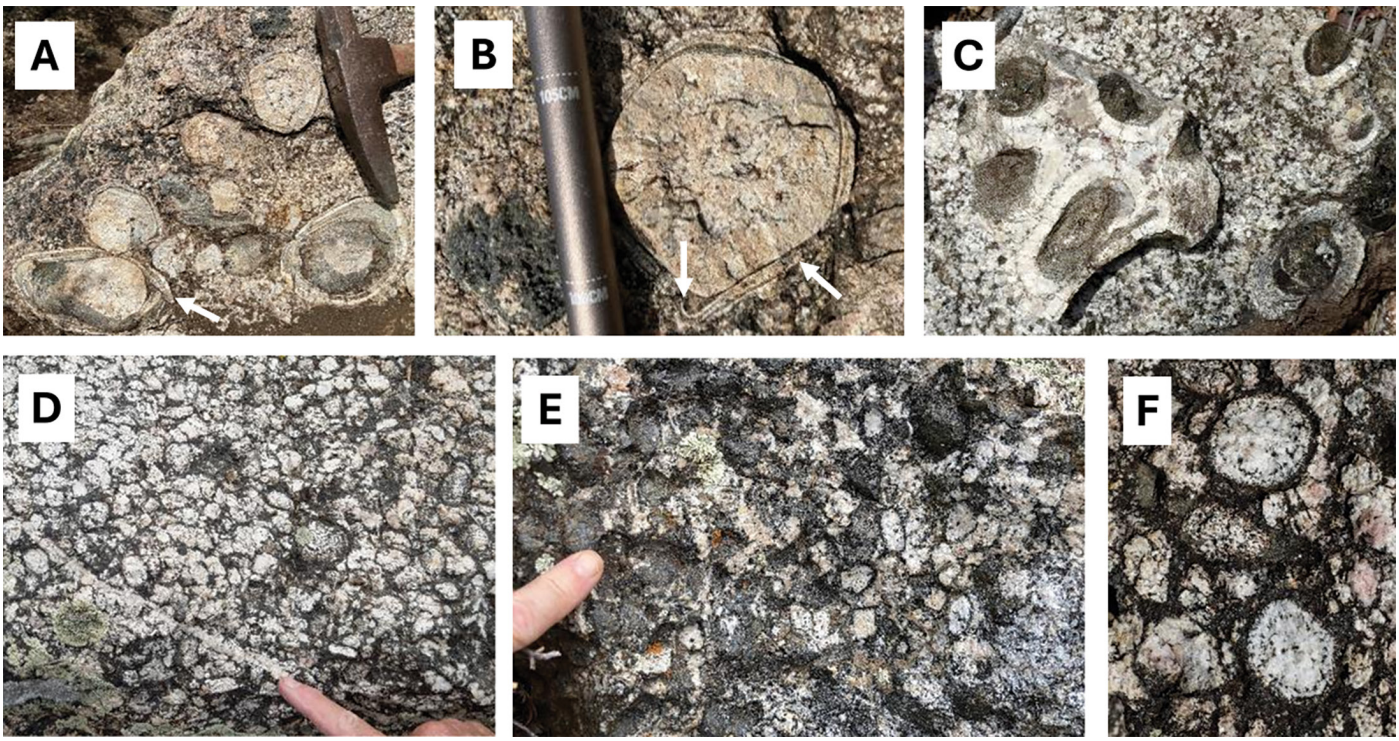


FIGURE 4. La Luz orbicules and host rock in outcrop. Host rock varies considerably in composition, texture, and mineralogy, suggesting that it is the product of incomplete magma mixing. Most large feldspars are rounded, with either biotite (Bt) or plagioclase (Plag) rims (proto-orbs of Enz, 1974). Typically, euhedral K-feldspar (Kfsp) megacrysts are sparse. A and B) Larger orbs with variable shell thicknesses; the orb at the hammer point is about 8 cm (3 in) in length; the orb next to the hiking stick is 5 cm (2 in); the increments on the hiking stick are 5 cm (2 in). One orb each in A and B has delaminated along the inner Bt shell (arrows). C) Smaller orbs in two samples, ranging from 2 to 5 cm (0.8–2.0 in), with prominent Bt-Plag shells. Larger block shows isolated orbs in monzodiorite host; smaller block shows tightly packed orbs with thick outer Plag shells (white) and IOM. D–F) Small orbs and proto-orbs (with single rounded feldspar megacryst as cores) with biotite and plagioclase shells. Intact Bt shells appear black (see finger). A thin aplite dike is present in D (see finger). E) shows host biotite monzodiorite with abundant small "proto-orbs" consisting of feldspar megacrysts, rimmed by Bt ± Plag. F) shows a close-up of proto-orbs with thick outer Bt shells.

Outcrops and textural relations indicate that the Sandia granite was intruded by small, possibly vertically oriented bodies of mQd and fQd, which were then cut by dikes of orbicular granite with an aplitic matrix between the orbs. A final stage of aplite dikes cuts the orbicular-bearing mass, followed by a much later stage of hydrothermal alteration, most noticeable within Sandia granite.

MINERALOGY AND MICROSCOPIC TEXTURAL RELATIONSHIPS

La Luz Orbicules

Textures of orbs and host rocks in thin section (32 mm [1.25 in] long dimension) and at the microscopic level are summarized in Figures 6–9. The main-phase Sandia granite is coarser-grained and contains more abundant and larger K-feldspar megacrysts, and significantly less biotite, than the hosting biotite ± amphibole monzodiorite (Figure 5, Table 1). The composition of wallrock at what appears to be the dike contact is lower in silica and higher in ferrous oxide (FeO_T) and MgO than samples of the main-phase granite analyzed by previous workers (see Appendix A; cf. Condie, 1978; Enz et al., 1979), suggesting that this sample is also part of a hybrid magma zone. Because large La Luz orbs were extensively altered, we examined smaller orbs in more detail. Small elliptical La Luz orbs with granitic cores and shells consisting of various proportions of biotite and plagioclase are shown in Figures 4 and 7. They consist of (1) a granitic core, (2) a concentric coarse-grained biotite rim, (3) an intergrown concentric-to-radial finer-grained biotite and radial plagioclase shell, and then (4) a strongly radial outer plagioclase shell surrounded by (5) inter-orb matrix. Minor amounts of quartz, K-feldspar, and accessory minerals, primarily titanite, are present in the shells. These same minerals, along with allanite, are more abundant in the inter-orb matrix, whereas biotite and plagioclase are less abundant.

Core minerals have normal interlocking granitic growth textures. Most cores are overgrown by a thick, coarse-grained layer of concentrically arranged biotite grains (BtS in Fig. 7).

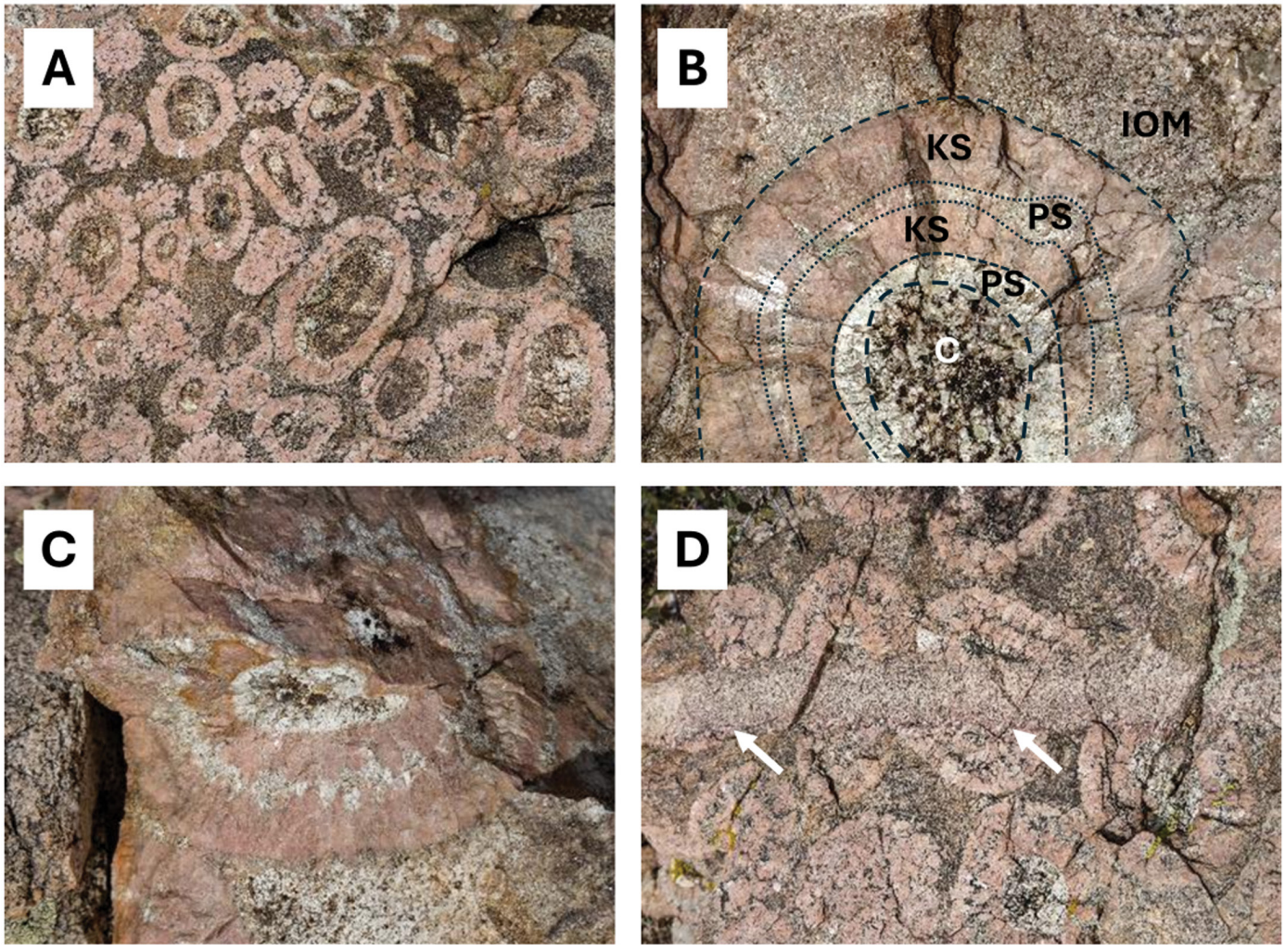


FIGURE 5. Tijeras Canyon orbicules and host rock in outcrop. A) Closely packed large orbs with relatively consistent shell thicknesses; the largest orb is ~14 cm (5.5 in) in the long dimension. B and C) Close-ups of large single orbs (~10–12 cm [4–5 in]) with granitic cores and a shell sequence of PS–KS–PS–KS. Shells are outlined with dashed lines in B): C = core; PS = Plag shell; KS = Kfsp shell; and IOM = inter-orb matrix. The outer PS is commonly thin, irregular, and discontinuous. D) Aplite dike cutting through closely packed orbicules (arrows). Note the similarity in grain size between the crosscutting aplite dike and the IOM.

Concentric biotite makes up ~70–90% of this layer, with lesser, radially oriented biotite grains and inclusions and interstitial plagioclase and minor quartz and titanite also present (Figs. 7A, 7C, 9C, and 9E). The high percentage of biotite, with less plagioclase and very little K-feldspar and quartz, suggests that this shell grew from a considerably more mafic magma than is represented by the core and by the bulk granodioritic composition of the Sandia pluton. Biotite grains are strongly elongate (with aspect ratios of 4:1–10:1). In fact, some concentric grains are so long that they have a significant arc of curvature parallel to the orb shape.

A series of finely intergrown minerals make up the next shell or shells (plagioclase–biotite) in Figure 7 (PBtS). These shells consist of approximately equal proportions of biotite and plagioclase (although either mineral may dominate in poorly defined sublayers) and vary in thickness. The biotite grains form local domains that share optical orientation, indicating that they form larger interconnected crystals in three dimensions. The prominent cleavage is concentric to the orb, whereas the fast direction (visible in cross-polarized light) of plagioclase growth is radial (perpendicular) to the orb axis.

In cross-polarized light, it is clear that radial plagioclase grew semicontinuously, accompanied sporadically by biotite, producing concentric layers and bands (Fig. 7B). Grosse et al. (2010) described very similar shells and suggested that this distribution of biotite in successive layers is a crystallization feature ruled by fluctuations of biotite saturation in the melt.

Outer shells are nearly monomineralic bladed plagioclase (PS in Fig. 7). Some plagioclase blades may be optically continuous across the PBtS and outer plagioclase layers, showing its dominance over biotite during this period of growth (Fig. 7B). This plagioclase layer is quite uniform from orb to orb in thickness and composition (Enz et al., 1979), with aspect ratios of 4:1–12:1. These textural and mineralogical variations are likely indicative of undercooled crystallization with fluctuations in magma composition and intensive parameters during shell formation.

Surrounding the orbicules, a texturally and mineralogically distinct IOM fills remaining space (Fig. 7A). It is fine-grained euhedral equigranular plagioclase and biotite locally encapsulated in larger K-feldspar. Myrmekite grew late, adjacent to K-feldspar, enclosing previously formed plagioclase and biotite indicating water saturation. Quartz is a minor constituent forming at feldspar grain boundaries and showing crenulated texture. It also forms fracture fillings in feldspars. Trace zircon, apatite, and allanite phases are present. Allanite is altered and has a partial rim of epidote locally (Fig. 9A). The IOM appears to have grown from the residual magma and fluid remaining after orb growth and has a more evolved chemical composition.

Tijeras Canyon Orbicules

The Tijeras occurrence forms a small hill and surrounding area near Tijeras Canyon in the southern Sandia Mountains (Affholter, 1979; Affholter and Lambert, 1982). Based on our reconnaissance mapping of current exposures, we concur with these earlier authors that the orbicular host rock is a pipelike body of two types of biotite–hornblende–quartz–monzodiorite within the main Sandia granite, and orbs are concentrated into two bands or dikes that may connect to the north (Fig.

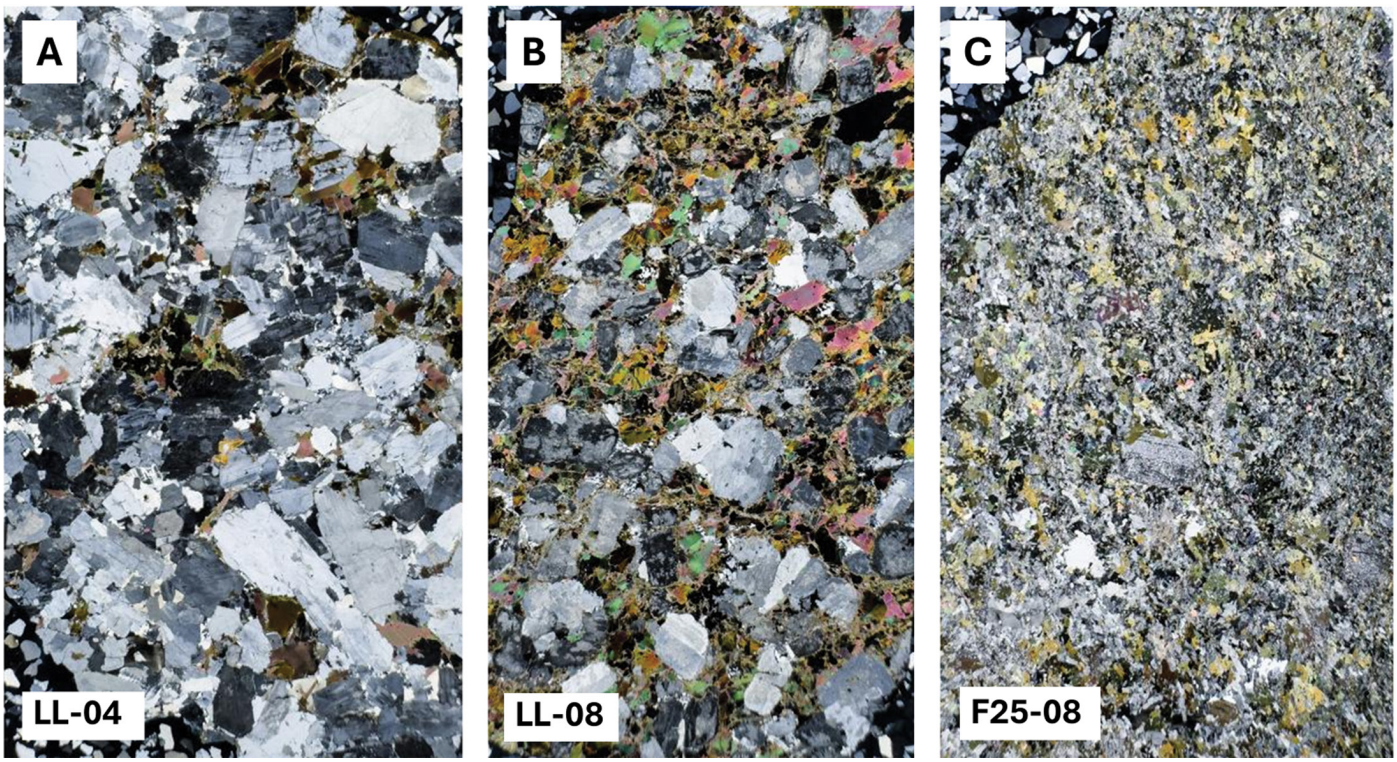


FIGURE 6. Orbicule host rocks in plane light and cross-polarized light. A) Diorite at orb dike contact. B) Biotite monzodiorite to gabbro hosting La Luz orbs. C) Biotite–hornblende monzodiorite hosting Tijeras Canyon orbs. Long dimension is ~3.2 cm (~1.3 in). See Table 1 for mineral abbreviations and modal estimates.

3). A fault and associated fine grained quartz–monzodiorite are found to the east, with main-phase Sandia granite in its hanging wall. Thin aplite dikes cut all intrusive phases and orbicules.

As described by Affholter (1979) and Affholter and Lambert (1982), "The orbicules, set in an aplite-pegmatite granitic matrix, have magmatic and metamorphic cores surrounded by a white plagioclase shell and one or two salmon-colored potassium-feldspar shells separated by a thinner, sometimes discontinuous plagioclase layer (Fig. 5). The outcrop occurs in two dike-like masses with thicknesses of 1–5 m (3–16 ft) trending N5°W and N35°E for exposed lengths of 16 m (52 ft) and 46 m (151 ft) and is surrounded by biotite syenodiorite and biotite monzonite." We term this rock quartz monzodiorite (see Fig. 3).

Figure 8 shows microtextural features of the orbicules, with an inner shell of plagioclase formed on core material, followed by a thicker shell of bladed K-feldspar. Outboard of the K-feldspar shell, finer IOM fills the remaining space.

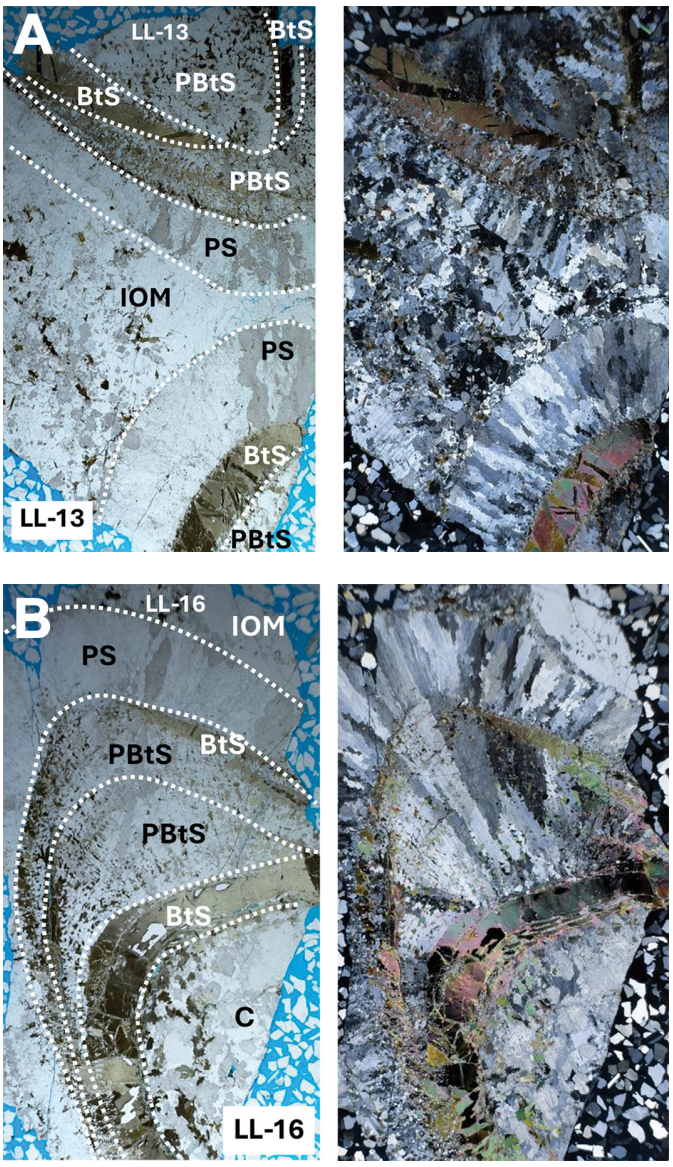


FIGURE 7. Petrography of La Luz orbs in plane light and cross-polarized light. A) Shells of two adjacent orbs and IOM. B) Small elliptical orb from core to outer PS. Long dimension is ~3.2 cm (~1.3 in). Abbreviations are in Figure 5 in addition: PBtS = Plag-Bt shell; BtS = Bt shell. Note strongly bladed plagioclase in shells.

Comparison of Occurrences

The Tijeras Canyon orbs are generally larger than those in the La Luz occurrence, with thick microcline (instead of biotite) shells alternating with plagioclase shells (cf. Figs. 4, 5, 7, and 8). The first shell is invariably plagioclase and the second shell microcline (plagioclase shell [PS] and K-feldspar shell [KS], respectively, in Fig. 8). This sequence is repeated in some orbs, with the microcline shells being thicker and more continuous than the plagioclase shells. Outer microcline shells are sometimes fractured, with inter-orbicular matrix penetrating the interstices (Affholter, 1979; Figure 8A). K-feldspar is less common than plagioclase in orbicular occurrences worldwide, but shells composed of intergrowths of the two feldspars with a mafic mineral have been documented.

Both Sandia orbicular occurrences are bounded in part by faults, which presumably formed after the system was completely solidified, but may signal that intrusion was initially localized by long-lived zones of structural weakness (Figs. 2 and 3). In both occurrences, shell minerals are strongly bladed (Figs. 7 and 9C). Also, both are located in more mafic intrusions of limited area, with local development of tightly packed orbicules of varying size, including proto-orbs (small orbs with a single megacryst as the core; Enz, 1974; Affholter, 1979).

Proto-orbs are typically K-feldspar, or plagioclase replacing K-feldspar, rimmed by biotite and/or plagioclase shells and akin to rapakivi granite in texture. In some cases, a rounded K-feldspar core remains, but in other cases, the K-feldspar is completely replaced by cellular textured plagioclase (Fig. 8B; cf. Stimac and Wark, 1992) that served as orb cores (also cf. Grosse et al., 2010). Rimming or replacement of K-feldspar by plagioclase may form when K-feldspar sourced from a silicic magma is immersed a hotter, more mafic magma because of mixing or mingling (Stimac and Wark, 1992; Wark and Stimac, 1992), although shifting phase relations attending rapid magma ascent (Nekvasil, 1991) and/or a decrease in magmatic water content related to loss of a volatile-phase (Cherry and Trembath, 1978) may also control their occurrence. Scenarios involving volatile loss from the top of a chamber with thermal replenishment from below could certainly involve a likely combination of these mechanisms.

The La Luz monzodioritic to gabbroic host rock shows more compositional variation and a higher content of mafic enclaves and surmicaceous enclaves than at the Tijeras Canyon occurrence. The orbicular shells also likely formed in an environment with higher K_2O and lower femic concentrations. Finally, the La Luz occurrence locality also has occurrences of comb layering, which have not been identified at Tijeras Canyon.

Mineralogy and Microtextures

Figure 9 documents several common mineralogical and textural features of the Sandia orbicular occurrences. Accessory

and trace phases are common in granitic rocks and act as repositories for incompatible elements, including rare earth elements (REE), high-field-strength elements (HFSE), and radioactive elements. The minerals titanite, zircon, apatite, and possibly rare monazite were noted as most abundant both in the main-phase quartz monzonite and in some orb cores and IOM. Titanite is commonly more abundant than Fe–Ti oxides (Table 1). Titanite and apatite were abundantly associated with biotite in La Luz biotite and plagioclase–biotite shells, whereas zircon was sparse and other trace phases were rare to absent (Fig. 9). Allanite, which to our knowledge has not previously been described from the Sandia intrusive complex, was observed in the main-phase quartz monzonite, some orb cores, and IOM.

We also noted that orbicular host rocks and IOM commonly showed a paragenesis whereby feldspars and mafic minerals crystallized first, but overlapped with later crystallizing quartz, titanite, Fe–Ti oxides, and trace phases. Quartz in particular encapsulated all other phases, commonly filling cavities with euhedral terminations of other phases (Fig. 9F). Although this is a common texture in granitic rocks, we take it as evidence that a vuggy porous network of open space allowed movement of either a water-rich magma or a silica-rich magmatic volatile phase up to the time of final crystallization. The lack of miarolitic cavities suggests this was a liquid rather than a vapor.

PETROCHEMISTRY

Based on whole-rock major and trace chemistry (Appendices A–C), the Sandia granite orbs and their host rocks (we did not analyze the main-phase Sandia granite) are peraluminous, subalkaline, high-calcium granitoids (Fig. 10A; Condie, 1978), and individual analyses display a typical calc-alkaline trend (Fig. 10B; Irvine and Baragar, 1971; Rollison, 1993). The Tijeras rocks are lower in Zr, Co, Cr, Ni, TiO_2, rare earth elements (Fig. 10C), and Hf, and higher in SiO_2, than the La Luz occurrence rocks with the exception of the Tijeras aplite dike, which is similar to the La Luz rocks. Pearce tectonic plots (Fig. 10D, 10E; Pearce et al., 1984) show that the Tijeras samples are akin to volcanic-arc granites, whereas the La Luz samples

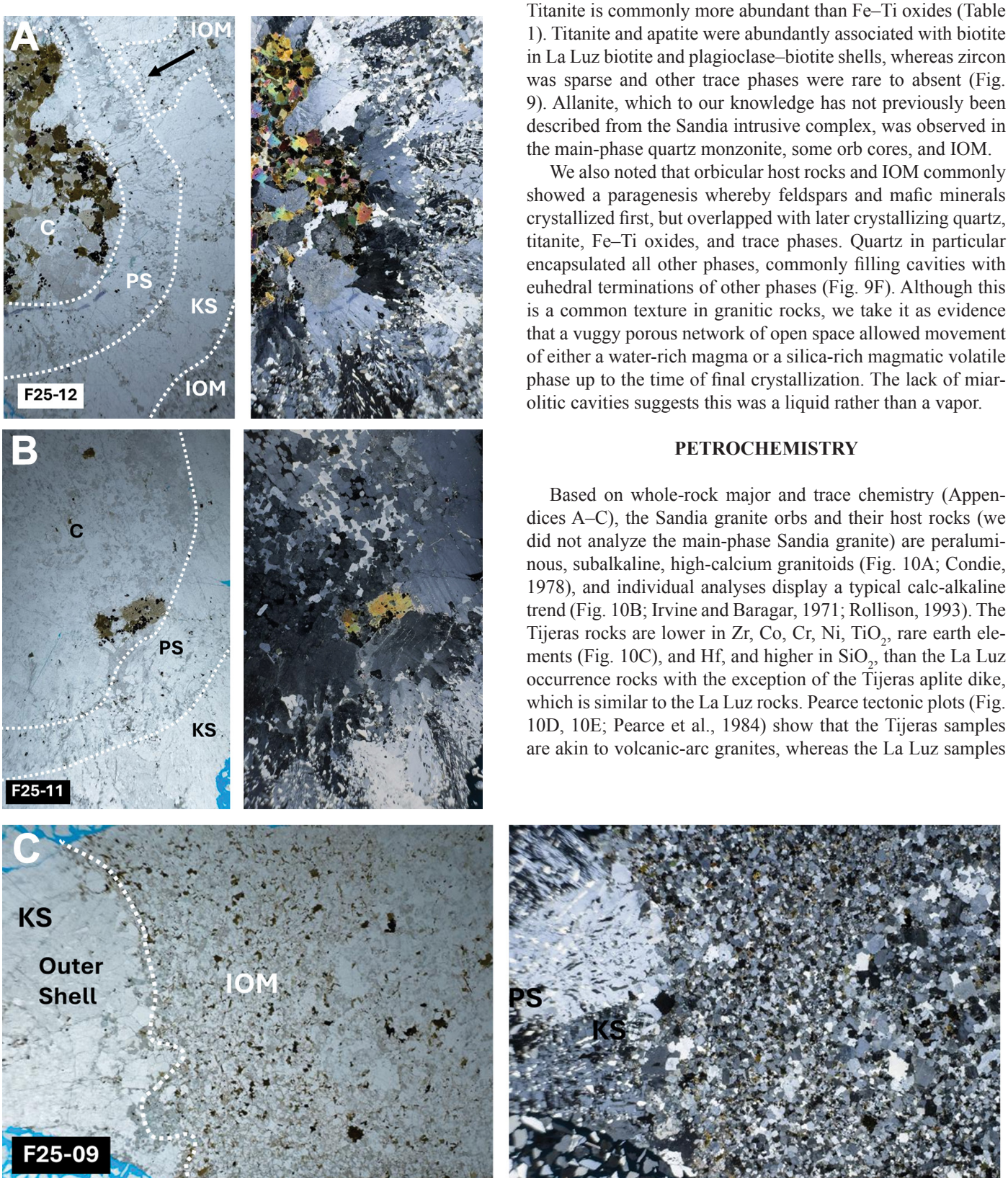


FIGURE 8. Petrography of the Tijeras Canyon orbs in plane light and cross polarized light. A) Orb from Bt-rich core to IOM that locally intruded outer K-feldspar shell (KS; arrow). B) Orb core mostly consisting of original potassium-felspar megacryst replaced or rimmed by cellular plagioclase overgrown by a plagioclase shell (PS) and KS. (C) Portion of orb consisting of outer KS and IOM. Long dimension is ~3.2 cm (~1.3 in). Abbreviations as in Figure 5

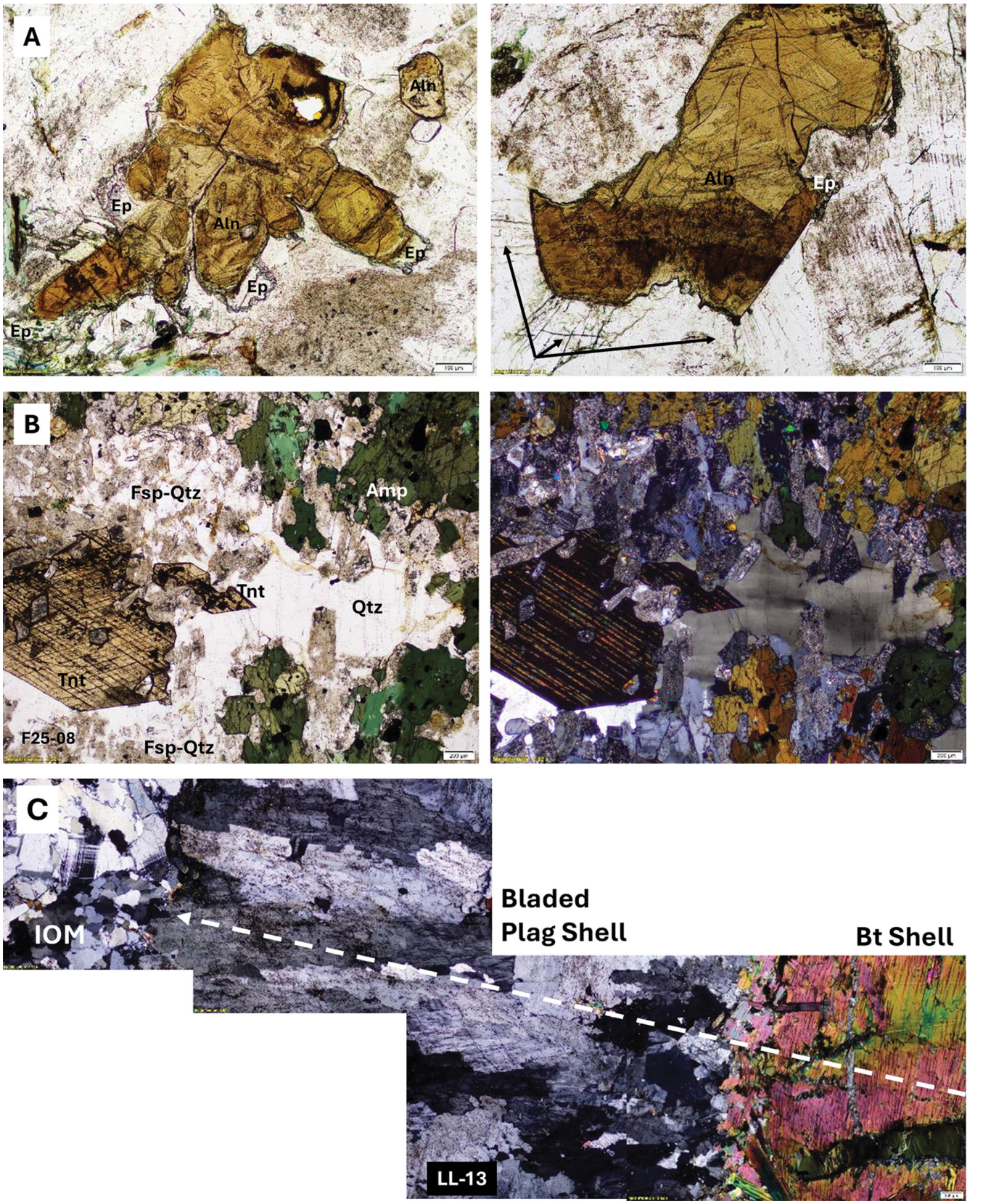


FIGURE 9. Mineralogy and microtextures of orbicules, host rocks, and inter-orb matrix (IOM) in plane-polarized (left) and cross-polarized light (right). A) Allanite (Aln) with thin rimming of epidote in Sandia Quartz Monzonite (LL04). Scale bars = 100 μm. Note radiation damage to the surrounding minerals (see arrows). B) Euhedral titanite–plagioclase–amphibole (Tnt–Plag–Amp) encapsulated in late quartz (Qtz) in Tijeras monzodiorite. Scale bars = 200 μm. C) Bladed plagioclase and K-feldspar (Kfsp) shells in La Luz (top, LL-13) and Tijeras Canyon orbs (bottom, F25-09), respectively. Scale bar = 200 μm. Bt = biotite.

are similar to within-plate granites, although our data are too limited to draw firm conclusions about this.

We compiled major-element chemistry data for both the main-phase Sandia granite and orbs and their hosting monzodiorite to gabbro (Enz, 1974, Enz et al., 1979; Condie and Budding, 1979; Affholter and Lambert, 1982; Majumdar, 1985) and compared them to our data (Fig. 10F, Appendix 1D). All but one sample previously classified as main-phase Sandia granite define tight arrays (dashed circles) indicating close genetic affiliation but showing no relationship to the orbs and their host rocks (traced by line with arrow). A crosscutting aplite also plots among the most evolved main-phase granites. Orb host rocks are considerably lower in SiO_2, higher in FeO_T, MgO, TiO_2 and P_2O_5, and similar in CaO and total alkalis relative to the main-phase granites. Their relatively linear trend over ~20wt% SiO_2 is characteristic of magma mixing. One sample, originally interpreted as main-phase Sandia granite, lies at the high-SiO_2 end of this trend and is probably associated with other orb host rock samples. Two orb cores (inherited resorbed granitoid rocks) also plot at slightly lower SiO_2 than the main-phase granite trend, but near the high-silica end of the orb host mixing trend except for P_2O_5.

Orbs (cores + shells) and orb shells scatter along the orb host mixing trend but are mostly located near its high-silica

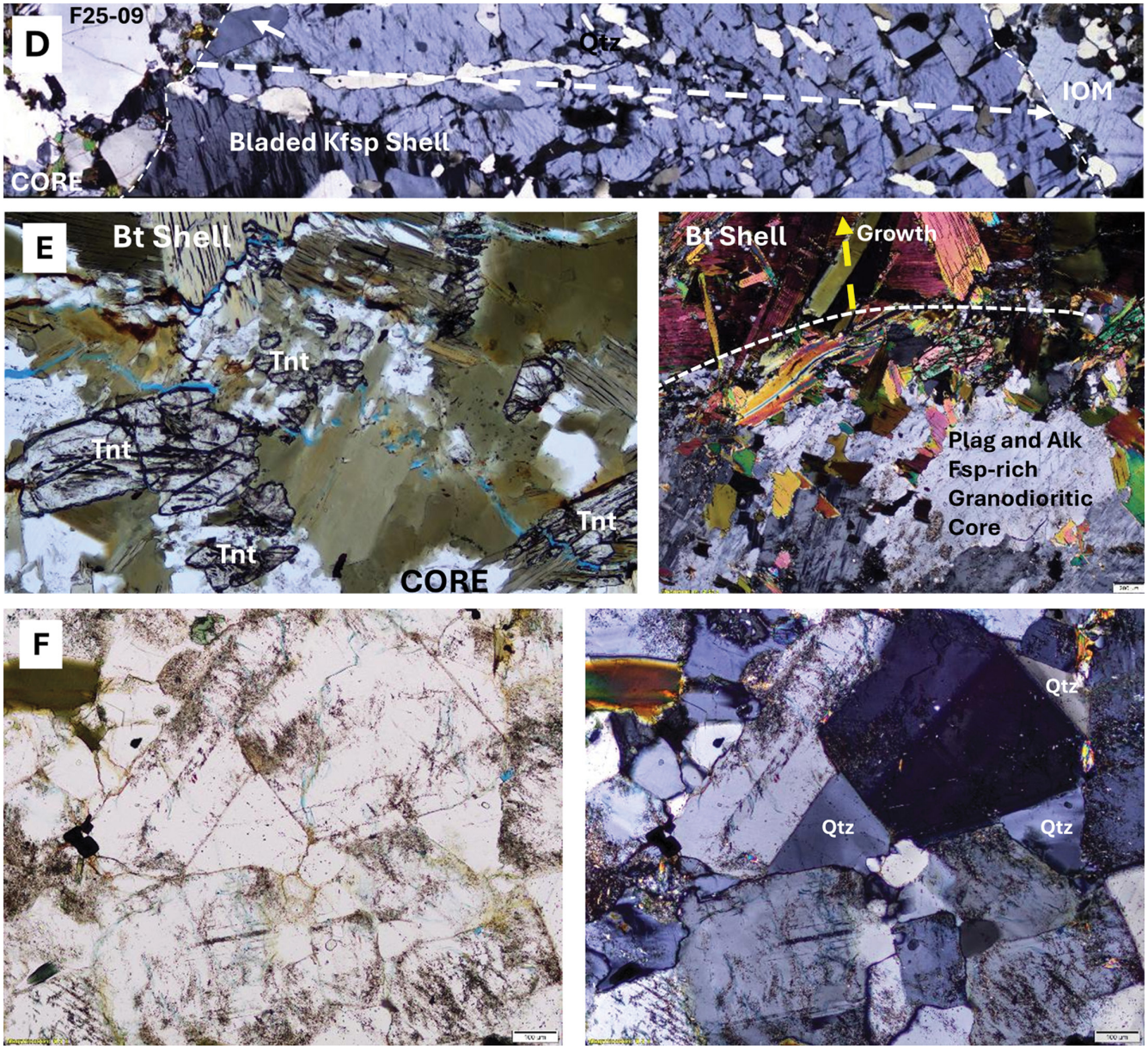


FIGURE 9 (continued). Mineralogy and microtextures of orbicules, host rocks, and inter-orb matrix (IOM) in plane-polarized (left) and cross-polarized light (right). Note radiation damage to the surrounding minerals. D) Bladed plagioclase and K-feldspar (Kfsp) shells in La Luz (top, LL-13) and Tijeras Canyon orbs (bottom, F25-09), respectively. The imaged area is 10 mm in length. E) Concentration of titanite (Tnt) at the contact of the resorbed core and the biotite (Bt) shell. Magnification on the left is slightly higher. Scale bars = 100 µm (left) and 200 µm (right), respectively. Alk = alkali; Fsp = feldspar. F) Close-up of IOM showing late-stage quartz (Qtz) infilling around euhedral plagioclase. Scale bar = 100 µm.

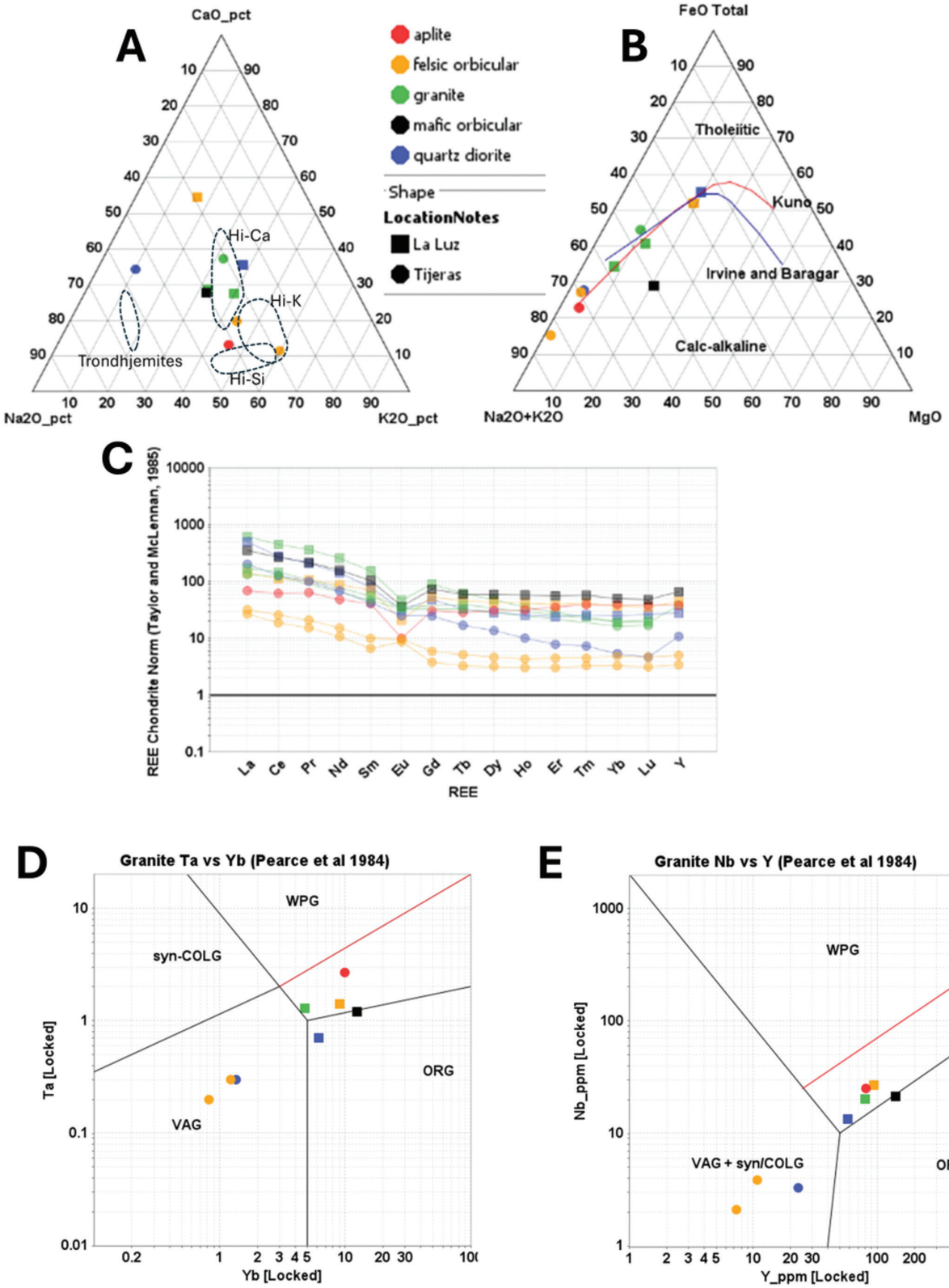


FIGURE 10. Major and trace element plots based on whole-rock chemical data of Sandia orbicular occurrences (data in Appendices A–C). A) Classification of Proterozoic granites (Condie, 1978). Symbol colors and shapes are the same for all plots. B) Atomic force microscopy (AFM) plot showing a typical calc-alkaline trend (blue line after Irvine and Baragar, 1971; red line after Kuno, 1968). C) Chondrite-normalized rare earth element (REE) plots (chondrite values from Taylor and McLennan, 1985). D) Tantalum versus ytterbium (Ta vs Yb) tectonic plot for granitic rocks (Pearce et al., 1984). Syn-COL = syn-collisional; WPG = within-plate granites; VAG = volcanic arc granites; and ORG = ocean-ridge granites. E) Niobium versus yttrium (Nb vs Y) tectonic plot for granitic rocks (Pearce et al., 1984). Abbreviations are as in D.

terminus at ~60wt% SiO_2. Orbs are also mostly off the main-phase Sandia granite trend, overlapping it only slightly at the highest SiO_2 values. They are more enriched in total alkalis (but lower in rare earth elements) than the granite and aplite, probably because they are composed mainly of feldspars. IOM plots along with orbs, ranging from ~60wt% to ~75wt% SiO_2.

These results are consistent with the orb host magma being distinct from the main-phase Sandia granite, having formed by hybridization of a mafic endmember with more evolved granitic material.

DISCUSSION

Analogs

The Sandia orb occurrences have much in common with other documented localities worldwide (e.g., Grosse et al., 2010; Smillie and Turnbull, 2014; Díaz-Alvarado et al., 2017; Zhang and Lee, 2020). The orbs from the La Luz occurrence bear a striking similarity to orbs described from the Sierra de Valasco, Argentina, described by Grosse et al. (2010). This locality consists of a restricted area of plagioclase and biotite-shelled orbs within a broader megacrystic granite pluton. The orbicular body has an irregular shape consisting of a main north–south-oriented segment of 65 m x 15 m (213 ft x 49 ft) and a smaller 35 x 5-m (115 ft x 16-ft) segment that branches out toward the northeast; however, the host rock is the main pluton, not a separate magmatic phase as at La Luz.

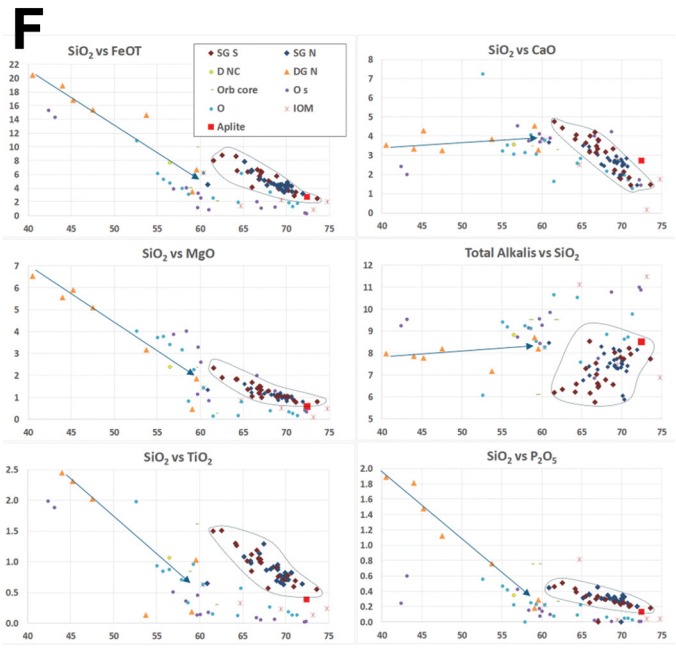


FIGURE 10 (continued). Major and trace element plots based on whole-rock chemical data of Sandia orbicular occurrences (data in Appendices A–C). F) Major-element plots for the main-phase Sandia granite, orbs, and their host rocks. SGS = Sandia granite south; SGN = Sandia granite north; DNC = diorite at orb-bearing dike contact north; DGN = diorite to gabbro orb host rock; O = orb; Os = orb shell(s); and IOM = inter-orb matrix. Dashed lines enclose an array of main-phase granite. Arrows show a linear mixing trend of orb host samples.

Both have proto-orbs in addition to larger orbs and orbicular accumulations.

Grosse et al. (2010) described ellipsoidal orbs (3–15 cm [1–6 in]) in an aplitic to pegmatitic matrix formed by a core made up of a K-feldspar megacryst, partially to totally replaced by plagioclase; an inner shell of radial and equant plagioclase crystals; a layer of tangentially oriented biotite laths; and an outer shell of plumose plagioclase crystals, containing diffuse rings of tangentially oriented biotite. Although radial crystallization of feldspar is normal in orbicules, tangential/concentric growth of biotite is also common, perhaps due to epitaxis (nucleation of a second mineral on an original mineral substrate replicating its crystal structure and orientation) controlled by the minimum interfacial energy achieved by crystal-lattice arrangements (Lahti, 2005; Sylvester, 2011).

The orbicular granitoid of Caldera, in the northern Chilean Coastal Range, has been described by Díaz-Alvarado et al. (2017) as another well-exposed example of orbs with radial textured shells. The orbs outcrop in a 375-m^2 tabular to lensoidal intrusive sheet emplaced in the compositionally diverse Lower Jurassic Relincho pluton. The orbicular structures are 3–7-cm (1–3 in)-diameter ellipsoids hosted in a porphyritic matrix. One contact with the host pluton shows a narrow zone of comb layering. The orbs have quartz–dioritic cores that are 3–5 cm (1–2 in) in diameter and composed of plagioclase ± hornblende + quartz + biotite ± K-feldspar, with a gabbroic shell, 2–3 cm (~1 in) in diameter, characterized by radiating plagioclase and hornblende. The shell crystals are bladed and oriented orthogonally to the core contact. The shell is in contact with the granodioritic IOM matrix through a 2–3-mm-wide poikilitic band around the orbicule that the authors term the outer shell. The outer shell and the matrix surrounding the orbicules contain large hornblende and biotite oikocrysts with inclusions of plagioclase and magnetite. The oikocrysts of both the outer shell and the IOM are elongate orthogonal to the radial inner shell. The coarse-grained granodioritic IOM matrix contains pegmatitic domains with large acicular hornblende and K-feldspar megacrysts.

Dikes and Pipes

The shapes of orbicular bodies are typically described as dikes, sheets, or pipes within larger plutons, reflecting their status as a late-stage intrusive phenomenon formed by brittle fracture of a solid pluton or destabilization of a rigid crystal mush; both sharp and gradational contacts are common. This is most readily achieved by a hotter, higher-pressure magma and is consistent with orbicules commonly occurring in a separate, more mafic intrusive phase (Smillie and Turnbull, 2014) or with mafic enclaves (Sylvester, 2011). Buoyancy may be achieved by higher temperatures and increasing volatile saturation as the intruding magma ascends.

In some cases, mafic enclaves formed as mafic magma or as a hybridized layer of intermediate magma, moved up and quenched into pillows along the flow path, and form a significant fraction of orb cores (Sylvester, 2011). In these occurrences, plagioclase and mafic minerals rapidly nucleated on some enclaves where the ascending magma interacted with a more felsic melt or aqueous fluid as it reached its final level of emplacement. In other cases where intrusion of a superheated mafic or hybrid magma is implicated, enclaves are rare, and the heat balance may have favored magma blending rather than mingling (Zhang and Lee, 2020).

If a crystal mush is being intruded by much hotter magma, some erosion and assimilation of mush components is likely and may contribute to the resorption of entrained crystals and partial dissolution of available core material. A large initial temperature difference (ΔT) is also likely to lead to strong undercooling and rapid crystallization once crystallization is initiated (Zheng and Lee, 2020). Some authors have inferred migration of residual water-rich magma or magmatic fluid from the crystal mush into the ascending plume or dike (e.g., Díaz-Alvarado et al., 2017), contributing to its volatile concentration.

Paterson (2009) described a granitic batholith with a wide variety of "pipes, diapirs, plume heads, and tubes" that crosscut each other and are thought to have flowed through preexisting crystal-rich magma or mush. He noted that these domains are rich in schlieren and mafic minerals, and inferred filter pressing and the accumulation of crystals of diverse origins and ages. The flow of hotter, more mafic magma through tubes and pipes, within more evolved crystal mush, might explain what Enz (1974) described as blending and/or interfingering of the host and intruding magmas along their interface.

Comb Layering

Comb layering commonly occurs with orbicular texture (Leveson, 1966; Moore and Lockwood, 1973; McCarthy and Müntener, 2016; Díaz-Alvarado et al., 2017). In most such occurrences, the main mineral precipitated is plagioclase, layered with biotite or amphibole. Comb layering involving mainly quartz is commonly referred to as unidirectional solidification texture (UST) by economic geologists (e.g., Lowenstern and Sinclair, 1996; Kirwin and Seltmann, 2002; Seo et al., 2021; Bain et al., 2022). They described USTs as consisting of repetitive layers of coarse-grained quartz that grow perpendicular to their respective substrate and are typically interlayered with fine-grained aplitic layers. Several studies have shown convincing evidence that quartz precipitates from a magmatic volatile phase or very water-rich magma at or near the top of an active magma body at temperatures of <800 °C (<1472 °F), whereas the aplitic layers were more clearly precipitated from magma. Open-system models for these occurrences entail fluctuations in the level of accumulated volatiles at the roof of a silicic magma body caused by episodic release of an aqueous fluid phase through a fractured carapace (Lowenstern and Sinclair, 1996; Kirwin and Seltmann, 2002; Seo et al., 2021; Bain et al., 2022). Fluid inclusion compositions and the presence of miarolitic cavities are consistent with the presence of a residual aqueous phase in many of these examples.

Müller et al. (2023) described some occurrences more compatible with a closed-system model. In a closed system, changes in pressure (and water content) cannot indefinitely shift phase boundaries because the residual melt fraction becomes depleted of the required elements, leading to mineral zoning and the growth of minerals enriched in the originally rejected elements. The repetition of plagioclase shells interspersed with either biotite or K-feldspar shells would most likely require movement of the orbs or differential flow of surrounding magma or fluid, resulting in changes in magma/fluid compositions. Flow would likely be stimulated by pluming or diking of the host magma to the location of orb formation.

Key Relationships and Orb Formation Mechanisms

As described above, most recent studies agree that orbicular texture forms during late-stage magmatic crystallization in granitoids, either from water-rich magma (Grosse et al., 2010; Smillie and Turnbull, 2014; McCarthy and Müntener, 2016; Díaz-Alvarado et al., 2017) or from a separated magmatic volatile phase (Moore and Lockwood, 1973; Sylvester, 2011). However, a complex sequence of events must occur for them to form. Most models for the formation of the radial textures of orbicular rocks involve several processes occurring in rapid succession: (1) superheating, (2) volatile exsolution, (3) undercooling, (4) geochemical fractionation, and (5) rapid crystallization of orb shells along with slower crystallization of IOM minerals (e.g., Díaz-Alvarado et al., 2017).

Like all occurrences, the Sandia orbs are complex, but Enz et al. (1979) and Affholter and Lambert (1982) concluded that "the orbicules appear to have formed by crystallization on available seed material (igneous and metamorphic rock) from a water- or vapor-rich segregation of the Sandia granite." However, Thompson and Giles (1974) inferred that late-stage metasomatism and/or hydrothermal processes formed the orbs.

Figure 11 illustrates our model for the orbicular occurrences documented in the Sandia pluton. It bears similarities to models proposed by other workers in which orbicules are hosted in a local, more mafic phase that has intruded a partially molten pluton (e.g., Sylvester, 2011; Smillie and Turnbull, 2014). The model shows a deep magma source region (Figs. 11A and 11B), a pipe or dike where the magma ascends through a semisolid or rigid crystal mush (Figs. 11C and 11D), a region of orb formation at a local roof or solidification front (Fig. 11E), and a zone of brittle fracture through the magma chamber carapace where volatiles escape to the hydrothermal realm above (Fig. 11F). Because orb formation most likely involves dynamic magma and volatile-phase flow over time and space, this diagram is an oversimplification. We describe the processes that contribute to orb formation from the bottom up in the next section.

Superheating/rock and mineral dissolution/reaction textures

Superheating and dissolution of entrained rock and mineral debris dominate in the magma source region and the deeper part of the pipe. A very hot superheated or crystal-poor magma may be one of the unusual requirements for orb formation. Vernon (1985) argued that the loss of crystal nuclei due to superheating leads to later undercooled crystallization and orbicular texture. In the case of magma ascent, heat loss and pressure drop associated with ascent and interaction with crystal mush on pipe walls would tend to increase undercooling of the crystal-poor magma as it reaches shallower levels.

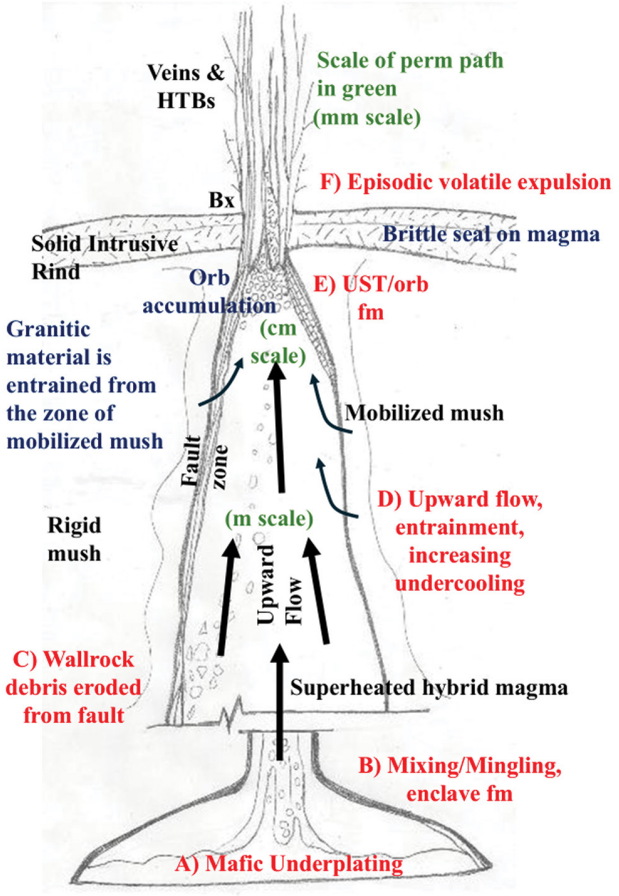


FIGURE 11. Model for orbicule formation in the Sandia pluton. A and B) At a deep level, mafic underplating generates volatile-rich, superheated hybrid (likely gabbroic to dioritic) magma that rises as a plume (pipe) or dike through semisolid crystal mush, assimilating and partially dissolving crystal mush and lesser wallrock. C and D) Wallrock is most likely from deep source regions, whereas crystal mush may be assimilated along the flowpath. The superheated magma ascends to the local chamber roof (D), where it is strongly volatile, oversaturated, and undercooled. E) Rapid crystallization occurs primarily on chamber walls and entrained crystalline and rock debris at a local chamber wall or roof zone, enhanced by strong undercooling and volatile loss. F) Overpressure from recharge, thermal buoyancy, and volatile saturation leads to fracturing of the chamber roof and episodic release of accumulated volatiles. Ascending flow during episodes of volatile release concentrates orbs upward, where they are captured in a solidification front. Multiple orb shells form in this environment on entrained solid debris that cannot pass upward through millimeter-scale fractures. Bx = breccia; HTB = hydrothermal breccia; fm = formation; UST = unidirectional solidification texture.

Most models that favor magmatic crystallization for orbicular texture involve the assimilation of adjacent rock or crystal mush to serve as core material within an otherwise superheated, crystal-poor magma. Once orb shells begin forming, crystallization is likely rapid (Smillie and Turnbull, 2014; Zheng and Lee, 2020). In the Sandia Mountains occurrences, the round and elliptical orb cores suggest dissolution occurred significantly before orb formation. Our favored mechanism for superheating is through underplating of mafic magma at the source region of the orb magma batch (Figs. 11A and 11B). This is a commonly invoked initiating mechanism for orbicular texture, although the exact scenarios differ (e.g., Sylvester, 2011; Smillie and Turnbull, 2014). In such cases, a superheated hybrid magma of intermediate composition, nearly devoid of seeds, is commonly produced. The hybrid magma may also include volatiles and quenched enclaves derived from the underplating magma. Large, partially dissolved clasts and enclaves are most likely to survive complete resorption.

Some disequilibrium mineral reaction textures associated with orb cores, such as the conversion of K-feldspar to cellular plagioclase, also develop as a result of the assimilation of K-feldspar megacrysts by the ascending mafic magma (see Stimac and Wark, 1992). Mineral textures indicate the formation of dissolution boundary layers and subsequent mineral growth within them. Orb shells in the La Luz occurrence contain a higher fraction of biotite than the core, suggesting crystallization from a more mafic magma composition, although it appears that the residual liquid becomes depleted of calcium and femic components with time, and the IOM is generally more evolved than the monzodiorite host.

Undercooling

Undercooled crystallization, resulting in rapid growth of elongate or bladed crystals, may be related to a decrease in temperature (i.e., temperature quenching), a decrease in pressure or in the partial pressure of water (P_{H2O}, pressure quenching), or both. Vernon (1985) argued that the elimination of seed crystals induced by high water concentration delays crystallization and results in significant undercooling. Initial superheating followed by undercooling of the melt has been proposed as a key mechanism for the formation of orbicular rocks (e.g., Vernon, 1985; Ort, 1992; Smillie and Turnbull, 2014). In the La Luz case, rapid ascent of the monzodiorite magma in a dike or pipe through cooler semi-rigid crystal mush would result in some hybridization (mush mobilization) and cooling. This would lead to the introduction of new seed material.

Díaz-Alvarado et al. (2017) speculated that the formation of orbicular texture (at the Caldera occurrence) may have been initiated during the generation of a magmatic fracture in the crystallization front (i.e., roof) of the Relincho pluton, where the water released by the host crystal mush was dissolved in the incoming batch of dioritic magma. Sylvester (2011) invoked a similar interaction between a more mafic incoming magma and its partially solid, more silicic host rock. Smillie and Turnbull (2014) even suggested that water might be released from metamorphism of country rocks in cases where the orbicules occur

near pluton margins. These mechanisms provide additional means of introducing water-rich fluids and inducing superheating, melt depolymerization, and resorption of existing crystals.

Orbicular and comb-layered rocks appear to form at the magma–hydrothermal interface, where water-rich magmatic fluids accumulated and episodically escaped from the carapace of the magma body. Late-stage overgrowths of epidote on allanite, titanite, and muscovite also formed as temperatures declined, either from residual magmatic fluid or from an ingress of meteorically sourced fluid. Diffuse copper mineralization present at the La Luz occurrence may provide further evidence of mediation by a magmatic volatile phase. The common occurrence of euhedral feldspars projecting into anhedral quartz suggests that vugs filled with late-stage magma or magmatic volatiles persisted until the final stages of solidification (Figs. 5–7). It is plausible that these cavities were connected in three dimensions, allowing migration of late-stage magmatic and even invading hydrothermal fluids until the final point of their infilling.

Late-stage quartz, filling cavities and encapsulating euhedral terminations of earlier formed minerals, may have crystallized from either a residual magmatic volatile phase or water-saturated silicate melt. Such a phase may have existed within a network of remaining cavities and had higher mobility than silicate melt by virtue of its low viscosity, even though the enclosing magma had reached a high degree of solidification. Overgrowths of epidote on allanite without an obvious time gap or fracture pathway are also consistent with the presence of a water-rich magma or a magmatic volatile phase at the final stage of solidification (e.g., Schmidt and Poli, 2004). Under these conditions, epidote is probably stable from ~550 °C to ~700 °C (~1022 °F to ~1292 °F), an unusually high formation temperature for epidote. Such a fluid may have controlled other late-stage solidification textures in the granite and modified earlier ones. Alternatively, epidote may have formed during a late-stage metasomatic phase at 250–450 °C (482–842 °F), as observed in metamorphic rocks (e.g., Stumpf et al., 2024). Future research on fluid inclusions might resolve these discrepancies in temperature formation and fluid phase composition.

USTs are characterized by successive, alternating bands of aplite and monomineralic quartz (with or without feldspar) with euhedral terminations that invariably point inward from the outer margin of the pluton. USTs of this composition are commonly interpreted as forming at the magmatic–hydrothermal transition as a result of repeated cycles of rupture and fluid loss. Such events are likely to form magmatic–hydrothermal breccias as fluid streams upward at high pressure. The mineral assemblage of orbicules and IOM is similar to that found in such hydrothermal breccias and veins associated with fluid expulsion from silicic to intermediate intrusions (feldspar–quartz–amphibole–[biotite]–epidote) commonly found in the deep upflow zones of geothermal systems (Stimac et al., 2015).

Volatile oversaturation and loss

Volatile oversaturation suppresses crystal nucleation, whereas volatile loss is commonly cited as leading to undercooling and rapid crystallization of the minerals that compose the orbicular shells (Ort, 1992; Grosse et al., 2010; Smillie and Turnbull, 2014). Volatile exsolution and loss can result from various processes. Two viable mechanisms that do not require transport of the "orbicular melt" are (1) water-pressure release associated with a volcanic eruption, as proposed by Ort (1992), and (2) fracturing of a mostly crystallized part of the wallrock and consequent degassing of the 'orbicular melt' (Grosse et al., 2010). Cycles of volatile loss and accumulation are vital to models of comb layering and UST.

Volatile overpressures may lead to the escape of an aqueous magmatic volatile phase through narrow fractures (Fig. 11). Changes in volatile pressure over time might lead to episodic accumulation and expulsion of fluids through the pluton carapace, common to many models of UST formation (e.g., Müller et al., 2023), but fracture aperture (typically millimeter scale) would limit the passage of orbicules, leading to their trapping and accumulation below fractures in the upper reaches of magmatic dikes and pipes.

CONCLUSIONS

Unusual and visually striking orbicular-textured rocks are known from hundreds of locations worldwide, but their origin has proven difficult to discern, and no universally accepted model exists. Clearly, a rather uncommon series of events was involved in their formation. Two occurrences of orbicular texture documented in the Sandia Mountains intrusive complex are concentrated in more mafic dike-like bodies that intrude into the main-stage Sandia quartz monzonite. Most modern studies attribute orbicular texture to complicated, late-stage magmatic processes involving some combination of magma mixing or segregation with episodic volatile oversaturation and expulsion at a local roof or magmatic solidification front (Fig. 11). These studies infer crystallization from a volatile-rich magma, but a few have also considered crystallization directly from a separated magmatic volatile phase (e.g., Moore and Lockwood, 1973; Sylvester, 2011). The link between comb layering at solidification fronts and associated orb accumulations has proved important for assessing their origins, as comb layering, or more generally UST, can clearly form from magmatic fluid.

Whatever the initiating sequence of events, orbicular shells appear to form at the magmatic–hydrothermal interface near the inferred top of the pluton. Our general model entails late-stage intrusion of hotter magma into a crystal mush near a local top of the intrusion, destabilizing the mush and ultimately leading to fracturing through the pluton roof and episodic expulsion of magmatic volatiles. We were unable to determine in our study whether orb shells form from water-rich magma or from an aqueous magmatic fluid, but either hypothesis is viable. Although there is ample compositional and textural evidence that mafic underplating at a deep level and mafic–felsic magma interaction at the level of emplacement played a significant role in the formation of the La Luz orbicular occurrence, this is less clear for the Tijeras Canyon site. Because our study was limited to field, textural, mineralogical, and chemical

relationships, we lack the detailed microanalytical or melt/fluid-inclusion evidence needed to narrow down the factors contributing to the formation of orbicular textures. Detailed fluid inclusion and mineral compositional patterns might allow further discrimination among the possible processes responsible for the origin of orbicular textures.

ACKNOWLEDGEMENTS

We are grateful to Kent Condie for his thoughtful review. Thin sections were made by Wagner Petrographics of Lindon, Utah. Esther Mandeno (Digital Mapping Solutions) is thanked for drafting maps. Our research was self-funded.

REFERENCES

Affholter, K., 1979, Petrogenesis of Orbicular Rock, Tijeras Canyon, Sandia Mountains, New Mexico [unpublished M.S. Thesis]: Albuquerque, University of New Mexico, 94 p. 3 app. https://digitalrepository.unm.edu/eps_etds/251

Affholter, K.A., and Lambert, E.E., 1982, Newly described occurrences of orbicular rocks in Precambrian granite, Sandia and Zuni Mountains, New Mexico: New Mexico Geological Society, Guidebook 33, p. 225–232. https//doi.org/10.56577/FFC-33

Bain, W.M., Lecumberri-Sanchez, P., Marsh, E.E., and Steele-MacInnis, M., 2022, Fluids and melts at the magmatic-hydrothermal transition, recorded by unidirectional solidification textures at Saginaw Hill, Arizona, USA: Economic Geology, v. 117, p. 1543–1571. https://doi.org/10.5382/econ geo.4952

Cherry, M.E., and Trembath, L.T., 1978, The pressure quench formation of rapakivi texture: Contributions to Mineralogy and Petrology, v. 68, p. 1–6. https://doi.org/10.1007/BF00375441

Condie, K.C., 1978, Geochemistry of Proterozoic granitic plutons from New Mexico, U.S.A.: Chemical Geology, v. 21, p. 131–149. https://doi.org/10.1016/0009-2541(78)90010-4

Condie, K.C., and Budding, A.J., 1979, Geology and geochemistry of Pre-Cambrian rocks, central and south-central New Mexico: New Mexico Bureau of Mines and Mineral Resources, Memoir 35, 58 p. https://doi.org/10.1016/0009-2541(78)90010-4

Díaz-Alvarado, J., Rodríguez, N., Rodríguez, C., Fernández, C., and Constanzo, I., 2017, Petrology and geochemistry of the orbicular granitoid of Caldera, northern Chile. Models and hypotheses on the formation of radial orbicular textures: Lithos, v. 284–285, p. 327–346. https://doi.org/10.1016/j.lithos.2017.04.017

Enz, R.D., 1974, Geochemistry and Petrology of the Orbicular Rocks, Sandia Mountains, New Mexico [unpublished M.S. Thesis]: Albuquerque, University of New Mexico, 73 p. https://digitalrepository.unm.edu/eps_etds/267/

Enz, R.D., Kudo, A.M., and Brookins, D.G., 1979, Igneous origin of the orbicular rocks of the Sandia Mountains, New Mexico: Geological Society of America Bulletin, v. 90, p. 349–380. https://doi.org/10.1130/GSAB-P2-90-349

Gaston, L.A., 2014, $^{40}Ar/^{39}Ar$ muscovite thermochronology and geochronology of New Mexico pegmatites [unpublished M.S. Thesis]: Socorro, New Mexico Institute of Mining and Technology, 139 p. https://www.ees.nmt.edu/outside/alumni/papers/2014t_gaston_la.pdf

Grambling, T.A., Karlstrom, K.E., Holland, M.E., and Grambling, N.L., 2016, Proterozoic magmatism and regional contact metamorphism in the Sandia-Manzano Mountains, New Mexico (U.S.A.): New Mexico Geological Society, Guidebook 67, p. 169–175. https://doi.org/10.56577/FFC-67.169

Grosse, P., Toselli, A.J., and Rossi, J.N., 2010, Petrology and geochemistry of the orbicular granitoid of Sierra de Velasco (NW Argentina) and implications for the origin of orbicular rocks: Geological Magazine, v. 147, p. 451–468. doi:10.1017/S0016756809990707

Holland, M.E., Grambling, T.A., Karlstrom, K.E., Jones, J.V., III, Nagotko, K.N., and Daniel, C.G., 2020, Geochronologic and Hf-isotope framework of Proterozoic rocks from central New Mexico, USA: Formation of the Mazatzal crustal province in an extended continental margin arc: Precambrian Research, v. 347, 820. https://doi.org/10.1016/j.precamres.2020.105820

Irvine, T.N., and Baragar, W.R.A., 1971, A guide to the chemical classification of the common volcanic rocks: Canadian Journal of Earth Sciences, v. 8, p. 523–548. https://doi.org/10.1139/e71-055

Kelly, V.C., and Northrop, S.A., 1975, Geology of Sandia Mountains and Vicinity, New Mexico: New Mexico Bureau of Mines and Mineral Resources, Memoir 29, p. 25–27. https://doi.org/10.58799/M-29

Kirby, E., Karlstrom, K.E., and Andronicos, C.L., 1995, Structural and thermal setting during emplacement of the Sandia Pluton, New Mexico Geological Society, Guidebook 46, p. 219–225. https://doi.org/10.56577/FFC-46.219

Kirwin, D.J., and Seltmann, R., eds., 2002, Extended abstracts: 11th Quadrennial International Association on the Genesis of Ore Deposits (IAGOD) Symposium and Geocongress, Geological Survey of Namibia, Windhoek, p. 22–26.

Kuno, H., 1968, Differentiation of basalt magma, *in* Hess, H.H. and Poldervaart, A., eds., Basalts: The Poldervaart Treatise on Rocks of Basaltic Composition: New York, Interscience Publishers, p. 623–688.

Lahti, S.I., ed., 2005, Orbicular Rocks in Finland, with contributions from Paul Raivio and Ilkka Laitakari: Geological Survey of Finland, 177 p.

Leveson, D.J., 1966, Orbicular rocks: A review: Geological Society of America Bulletin, v. 77, p. 409–426. https://doi.org/10.1130/0016-7606(1966)77[409:ORAR]2.0.CO;2

Lowenstern, J.B., and Sinclair, W.D., 1996, Exsolved magmatic fluid and its role in the formation of comb-layered quartz at the Cretaceous Logtung W-Mo deposit, Yukon Territory, Canada: Transactions of the Royal Society of Edinburgh, v. 87, p. 291–303. https://doi.org/10.1017/S0263593300006696

Majumdar, A., 1985, Geochronology, geochemistry and petrology of the Precambrian Sandia Granite, Albuquerque, New Mexico [unpublished Ph.D. Thesis]: Baton Rouge, Louisiana State University, 212 p. https://repository.lsu.edu/gradschool_disstheses/4061

McCarthy, A., and Müntener, O., 2016, Comb layering monitors decompressing and fractionating hydrous mafic magmas in subvolcanic plumbing systems (Fisher Lake, Sierra Nevada, USA): Journal of Geophysical Research, Solid Earth, v. 121, 12. https://doi.org/10.1002/2016JB013489

Moore, J.G., and Lockwood, J.P., 1973, Origin of comb layering and orbicular structure, Sierra Nevada batholith, California: Geological Society of America Bulletin, v. 84, no. 1, p. 1–20. https://doi.org/10.1130/0016-7606(1973)84%3C1:OOCLAO%3E2.0.CO;2

Müller, A., Kirwin, D., and Seltmann, R., 2023, Textural characterization of unidirectional solidification textures related to Cu–Au deposits and their implication for metallogenesis and exploration: Mineralium Deposita, v. 58, p. 1211–1235. https://doi.org/10.1007/s00126-023-01175-x

Nekvasil, H., 1991, Ascent of felsic magmas and formation of rapakivi: American Mineralogist, v. 76, p. 1279–1290.

Ort, M.H., 1992, Orbicular volcanic rocks of Cerro Panizos: their origin and implications for orb formation: Geological Society of America Bulletin, v. 104, p. 1048–1058. https://doi.org/10.1130/0016-7606(1992)104%3C1048:OVROCP%3E2.3.CO;2

Paterson, S.R., 2009, Magmatic tube, pipes, troughs, diapirs, and plumes: Late-stage convective instabilities resulting in compositional diversity and permeable networks in crystal-rich magmas of the Tuolumne batholith, Sierra Nevada, California: Geosphere, v. 5, p. 496–527. https://doi.org/10.1130/GES00214.1

Pearce, J.A., Harris, N.B.W., and Tindle, A.G., 1984, Trace element discrimination diagrams for the tectonic interpretation of granitic rocks: Journal of Petrology, v. 24, p. 956–983. https://doi.org/10.1093/petrology/25.4.956

Rollison, H.R., 1993, Using Geochemical Data: Evaluation, Presentation, Interpretation: London, Taylor and Francis Group, 384 p. https://doi.org/10.4324/9781315845548

Schmidt, M.W., and Poli, S., 2004, Magmatic epidote, *in* Liebscher, A., & Franz, G., eds., Epidotes: Reviews in Mineralogy and Geochemistry: Mineralogical Society of America, v. 56, pp. 399–430. https://doi.org/10.1515/9781501509599-012

Shomaker, J.W., 1965, Geology of the southern portion of the Sandia Granite, Sandia Mountains, Bernalillo County, New Mexico [unpublished M.S. Thesis]: Albuquerque, University of New Mexico, 80 p.

Seo, J.H., Kim, Y., Lee, T., and Guillong, M., 2021, Periodically released magmatic fluids create a texture of unidirectional solidification (UST) in Ore-forming granite: A fluid and melt inclusion study of W-Mo forming Sannae-Eonyang granite, Korea: Minerals, v. 11, 888. https://doi.org/10.3390/min11080888

Smillie, R.W., and Turnbull, R.E., 2014, Field and petrographical insight into the formation of orbicular granitoids from the Bonney Pluton, southern Victoria Land, Antarctica: Geological Magazine, v. 151, no. 3, p. 534–549. https://doi.org/10.1017/S0016756813000484

Stimac, J.A., and Wark, D.A., 1992, Plagioclase mantles on sanidine in silicic lavas, Clear Lake, California: Implications for the origin of rapakivi texture: Geological Society of America Bulletin, v. 104, p. 728–744. https://doi.org/10.1130/0016-7606(1992)104<0728:PMOSIS>2.3.CO;2

Stimac, J.A., Goff, F., and Goff, C.J., 2015, Intrusion-related geothermal systems, *in* Sigurdsson, H., Houghton, B., McNutt, S.R., Rymer, H., and Stix, J., eds., The Encyclopedia of Volcanoes, 2nd edition: Amsterdam, Academic Press, p. 799–822. https://doi.org/10.1016/B978-0-12-385938-9.00046-8

Stumpf, S., Skrzypek, E., and Stüwe, K., 2024, Dating prograde metamorphism: U-Pb geochronology of allanite and REE-rich epidote in the Eastern Alps: Contributions to Mineralogy and Petrology, v. 179, 63. https://doi.org/10.1007/s00410-024-02130-3

Sylvester, A.G., 2011, The nature and polygenetic origin of orbicular granodiorite in the Lower Castle Creek pluton, northern Sierra Nevada batholith, California: Geosphere, v. 7, no. 5, p. 1134–1142. https://doi.org/10.1130/GES00664.1

Taylor, S.R., and McLennan, S.M., 1985, The Continental Crust: Its Composition and Evolution: Oxford, Blackwell Scientific Publications, 312 p.

Thompson, T.B., and Giles, D.L., 1974, Orbicular rocks of the Sandia Mountains, New Mexico: Geological Society of America Bulletin, v. 85, p. 911–916. https://doi.org/10.1130/0016-7606(1974)85<911:OROTSM>2.0.CO;2

Vernon, R.H., 1985, Possible role of superheated magma in the formation of orbicular granitoids: Geology, v. 13, p. 843–845. https://doi.org/10.1130/0091-7613(1985)13<843:PROSMI>2.0.CO;2

Wark, D.A., and Stimac, J.A., 1992, Origin of mantled (rapakivi) feldspars: experimental evidence of a dissolution- and diffusion-controlled mechanism: Contributions to Mineralogy and Petrology, v. 111, p. 345–361. https://doi.org/10.1007/BF00311196

Zhang, J., and Lee, C.-T.A., 2020, Disequilibrium crystallization and rapid crystal growth: a case study of orbicular granitoids of magmatic origin: International Geology Review, v. 63, no. 7, p. 900–916. https://doi.org/10.1080/00206814.2020.1734975

Appendices can be found at
https://nmgs.nmt.edu/repository/index.cfml?rid=2026010



Orbicular granite in the Sandia Mountains. Photograph courtesy of Stan Davis.